

**The role of auditory sensory input during functional pre-
and postsynaptic maturation of the calyx of Held synapse**

PhD Thesis

in partial fulfilment of the requirements
for the degree “Doctor of Philosophy (PhD)/Dr. rer. nat.”
in the Neuroscience Program
at the Georg August University Göttingen,
Faculty of Biology

submitted by

Emilio Erazo Fischer

born in

Punta Arenas, Chile

2006

Herewith I declare, that I prepared the PhD Thesis

'The role of auditory sensory input during functional pre- and postsynaptic maturation of the calyx of Held synapse'

on my own and with no other sources and aids than quoted.

Göttingen, Sept. 18th 2006

.....

(Emilio Erazo Fischer)

To my beloved Natalia

And my dear parents

LIST OF CONTENTS

List of Contents	5
1 Introduction	7
1.1 Synaptic transmission at chemical synapses	8
1.2 Developmental plasticity in the central nervous system	10
1.3 The calyx of Held synapse.....	12
1.4 Developmental maturation at the calyx of Held synapse.....	16
1.4.1 Presynaptic changes	16
1.4.2 Postsynaptic changes.....	18
1.4.3 Short-term plasticity	19
1.5 Aim of this study.....	20
2 Materials and Methods	23
2.1 Slice preparation	23
2.2 Electrophysiology	25
2.3 Data analysis.....	28
3 Results	31
3.1 Synaptic transmission in $Ca_v1.3^{-/-}$ synapses	31
3.2 Presynaptic action potentials of $Ca_v1.3^{-/-}$ mice during trains	34
3.3 Presynaptic Ca^{2+} currents and exocytosis in calyceal terminals from $Ca_v1.3^{-/-}$ mice	36
3.4 Presynaptic AP waveform in $Ca_v1.3^{-/-}$ mice.....	41
3.5 Enhanced synaptic strength in $Ca_v1.3^{-/-}$ mice.....	44
3.6 Elevated release probability in calyx of Held synapses of $Ca_v1.3^{-/-}$ mice.....	51
3.7 Delayed down-regulation of synaptic NMDA receptors in $Ca_v1.3^{-/-}$ mice	61
4 Discussion	69
4.1 Synaptic transmission is intact in mature $Ca_v1.3^{-/-}$ calyx of Held-MNTB synapses.....	71
4.2 Developmental refinement of presynaptic properties in the absence of afferent nerve activity	72
4.3 The level of afferent nerve activity regulates release probability.....	73

4.4 Postsynaptic AMPA and NMDA receptors show different sensitivity to chronic changes in afferent nerve activity	78
4.4.1 AMPA receptors are not affected by reduced levels of activity	78
4.4.2 NMDA receptors are regulated by afferent nerve activity.....	79
4.5 Comparison to in vitro studies.....	80
5 Summary	84
References	85
Acknowledgments.....	97
Curriculum Vitae.....	98
List of Publications	99

1 INTRODUCTION

The nervous system is a network that contains billions of individual nerve cells interconnected in systems that construct our perceptions of the external world, fix our attention, and control the machinery of our actions. A first step toward understanding how it works, therefore, is to learn how neurons are organized into signaling pathways and how they communicate.

Neurons communicate through specialized zones of contact called the *synapse*, a term that was introduced more than 100 years ago by Charles Sherrington (1906). This term was later adopted by Ramón y Cajal (1911), who was the first to describe this site morphologically, at the level of light microscopy. Once the fine structure of synapses was made visible with the electron microscope, it was possible to distinguish that, in chemical synapses, neurons are separated completely by a small space, the *synaptic cleft* (Pappas et al., 1972). There is no continuity between the cytoplasm of one cell and the next. As a result, chemical synaptic transmission depends on the release of a *neurotransmitter* from the presynaptic neuron. A neurotransmitter is a chemical substance that will bind to specific receptors in the postsynaptic cell membrane. Neurotransmitters are stored in membranous structures called *synaptic vesicles*, which in turn are contained in specialized swellings of the axon, the *presynaptic terminals*. Synaptic vesicles cluster at regions of the membrane specialized for transmitter release called *active zones*, where synaptic vesicle proteins undergo several structural modifications before actual fusion may occur (Sudhof, 2004).

Several questions have arisen from the visualization of these distinct structures. For example, how is an electrical signal transformed into a chemical one, and then back again to electrical transmission in the postsynaptic cell? Which synaptic elements play part in this process? And more important, what are the detailed steps of synaptic transmission? These few questions will be answered in the next section.

1.1 Synaptic transmission at chemical synapses

Commonly, processing and modulation of information takes place at the synapse, where electrically propagated signals across a neuron arrive often, in form of an action potential (AP). An AP is converted into a chemical signal at the presynaptic terminal, through several steps lasting around 0.8 ms (Sudhof, 2004), Fig. 1).

During discharge of a presynaptic AP, voltage-gated Ca^{2+} channels at active zones open at elevated membrane potentials (Fig. 1, step 1), causing the flux of Ca^{2+} into the presynaptic terminal due to a gradient between a low intracellular and a high extracellular Ca^{2+} concentration. The rise in intracellular Ca^{2+} concentration is sensed by a Ca^{2+} sensor attached to synaptic vesicles. The binding of Ca^{2+} to this sensor decreases, through complex steps, the energy barrier for vesicle fusion. Thereby, the probability of transmitter release is dramatically increased and vesicles fuse with the membrane (Fig. 1, step 2).

Neurotransmitter molecules released into the extracellular space diffuse across the synaptic cleft and bind to their receptors on the postsynaptic cell membrane (Fig. 1, step 3). This in turn activates the receptors, leading to the opening of ion channels. In the case of excitatory ionotropic neurotransmitters, activated

receptor molecules will open pores which allow for cation flux into the cell, increasing transiently the membrane potential of the postsynaptic cell.

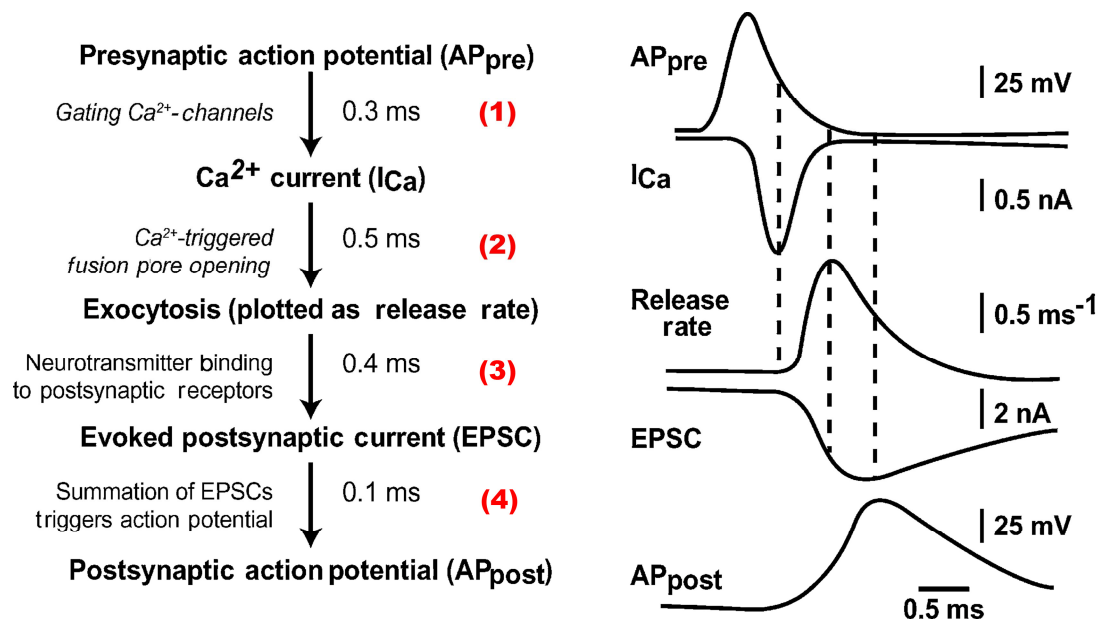


Figure 1. Steps sequence and timing of chemical synaptic transmission

The principal steps with the associated time constants are shown on the left, and traces from the corresponding steps in the calyx of Held synapses are illustrated on the right (Meinrenken et al., 2003). An action potential arriving at the presynaptic terminal of an axon causes voltage-gated Ca²⁺ channels at the active zone to open (1). The influx of Ca²⁺ produces a high concentration of Ca²⁺ near the active zone, which in turn causes vesicles containing neurotransmitter to fuse with the presynaptic cell membrane and release their contents into the synaptic cleft (2) (Exocytosis). The released neurotransmitter molecules then diffuse across the synaptic cleft and bind to specific receptors on the postsynaptic membrane (3). These receptors cause ion channels to open (or close), thereby changing the membrane conductance and membrane potential of the postsynaptic cell (4). *Right panel*, the complex process of chemical transmission is responsible for the delay between action potentials in the pre- (AP_{pre}) and postsynaptic (AP_{post}) cells. Modified from Südhof (2004).

In this way, the chemical signal is reconverted into an electrical signal as an excitatory postsynaptic potential (EPSP). If threshold is reached by temporal and/or spatial summation, a new postsynaptic action potential is elicited (Fig. 1, step 4). This newly generated AP may propagate through the neuron to finally

arrive at the next synaptic connection. The most abundant excitatory neurotransmitter in the central nervous system (CNS) of mammals is (L)-glutamate which binds to postsynaptic ionotropic glutamate receptors of AMPA-, kainate and/or NMDA-type.

After summarizing the steps of synaptic transmission, obvious questions emerge. For example, how synaptic properties change during development? Moreover, which are the forces that drive developmental plasticity, and which processes of synaptic communication are more inclined to undergo these changes? For the last 30 years, our knowledge in the mechanisms of synaptic transmission has steadily increased, but the role of afferent activity during the development of synapses remains unclear. The next section briefly introduces recent studies on how nerve activity influences synaptic properties in CNS neurons, and discusses shortly the limitations presented by the chosen models.

1.2 Developmental plasticity in the central nervous system

The morphological and functional refinement of synapses in the mammalian CNS during early postnatal development is controlled by a collection of genetic and epigenetic factors. Nerve activity and neurotransmitter release may serve epigenetic functions by promoting or inhibiting synaptogenesis (Kirov and Harris, 1999; Marty et al., 2000; 2004), regulating the pattern of innervation (Chattopadhyaya et al., 2004) and decreasing or increasing the strength of synaptic connections (Turrigiano et al., 1998; Murthy et al., 2001; Thiagarajan et al., 2005). This regulation is achieved by modulating expression, trafficking, degradation and function of a variety of synaptic proteins (Rao and Craig, 1997; O'Brien et al., 1998; Ehlers, 2000; Mu et al., 2003; Townsend et al., 2004; Wilson et al., 2005).

One homeostatic mechanism that modulates synaptic strength is referred to as synaptic scaling. The term has emerged from recent studies in mammalian cortical synapses. If the average firing rate of a neuron *decreases*, then the system will *scale up* the excitatory and *scale down* the inhibitory inputs to that neuron, so it can reach previous levels of excitation (Burrone and Murthy, 2003; Turrigiano and Nelson, 2004; Thiagarajan et al., 2005). This change in synaptic strength may occur as a change in the number of synaptic contacts (within neural networks), a change in presynaptic release and/or in postsynaptic responses to transmitter release.

Depending on the type of synapse and experimental conditions under study, manipulation of neuronal activity resulted in a variety of effects in the properties and locus where these changes occur. Some examples of the remodeling of neuronal excitability are quantal size modification attributed to changes in postsynaptic receptors (Turrigiano et al., 1998) or the amount of neurotransmitter packed into synaptic vesicles (presynaptic changes) (Wilson et al., 2005). Other studies showed changes in quantal content without variation in quantal size (Bacci et al., 2001) or alterations in synaptic dimensions (Murthy et al., 2001). Desai et al. (1999) showed that a reduction of activity in response to TTX application in visual cortex neurons, leads to a down-regulation of potassium currents and an up-regulation of sodium currents with a concomitant increase in cell excitability. Synaptic scaling may occur preferentially in neuronal networks, where hundreds of excitatory and inhibitory synapses act together to achieve stable activity patterns (Turrigiano and Nelson, 2004). However, one restraint using neuronal networks is the open question if a similar phenomenon occurs at single synaptic connections.

Moreover, in contrast to the wealth of data describing multiple effects of

pharmacologically silencing activity on synaptic transmission *in vitro*, little is known about the consequences of chronically changing the levels of physiological activity on synapses developing *in-vivo* (Vale and Sanes, 2000; Tian and Copenhagen, 2001; Oleskevich and Walmsley, 2002; Clem and Barth, 2006). On the other hand, only few studies focused on afferent nerve activity driven development, at the level of isolated individual synapses (Oleskevich and Walmsley, 2002; Oleskevich et al., 2004; Youssoufian et al., 2005). Furthermore, because of the small size of the majority of presynaptic endings in the mammalian CNS, it is very difficult or impossible to directly assess presynaptic properties. To overcome these limitations, we address the above mentioned question, in a giant glutamatergic synapse of the auditory brainstem, the calyx of Held.

1.3 The calyx of Held synapse

As mention before, the size of a synapse is a significant technical constraint for electrophysiological recording. Substantial insight into synaptic function has been provided by exploiting the large dimensions of several model synapses. For instance, Katz (1969) used the frog neuromuscular junction to first demonstrate that neurotransmitter release occurs in discrete quanta, indicating that transmitter is stored in packages of specific size, later known as synaptic vesicles. In another large model, the giant squid stellate ganglion, a direct relation between presynaptic Ca^{2+} currents and postsynaptic membrane potentials was directly quantified (Llinas et al., 1981). However, the progress of studies in the CNS was long restricted by the technical difficulty of presynaptic recording from small nerve terminals.

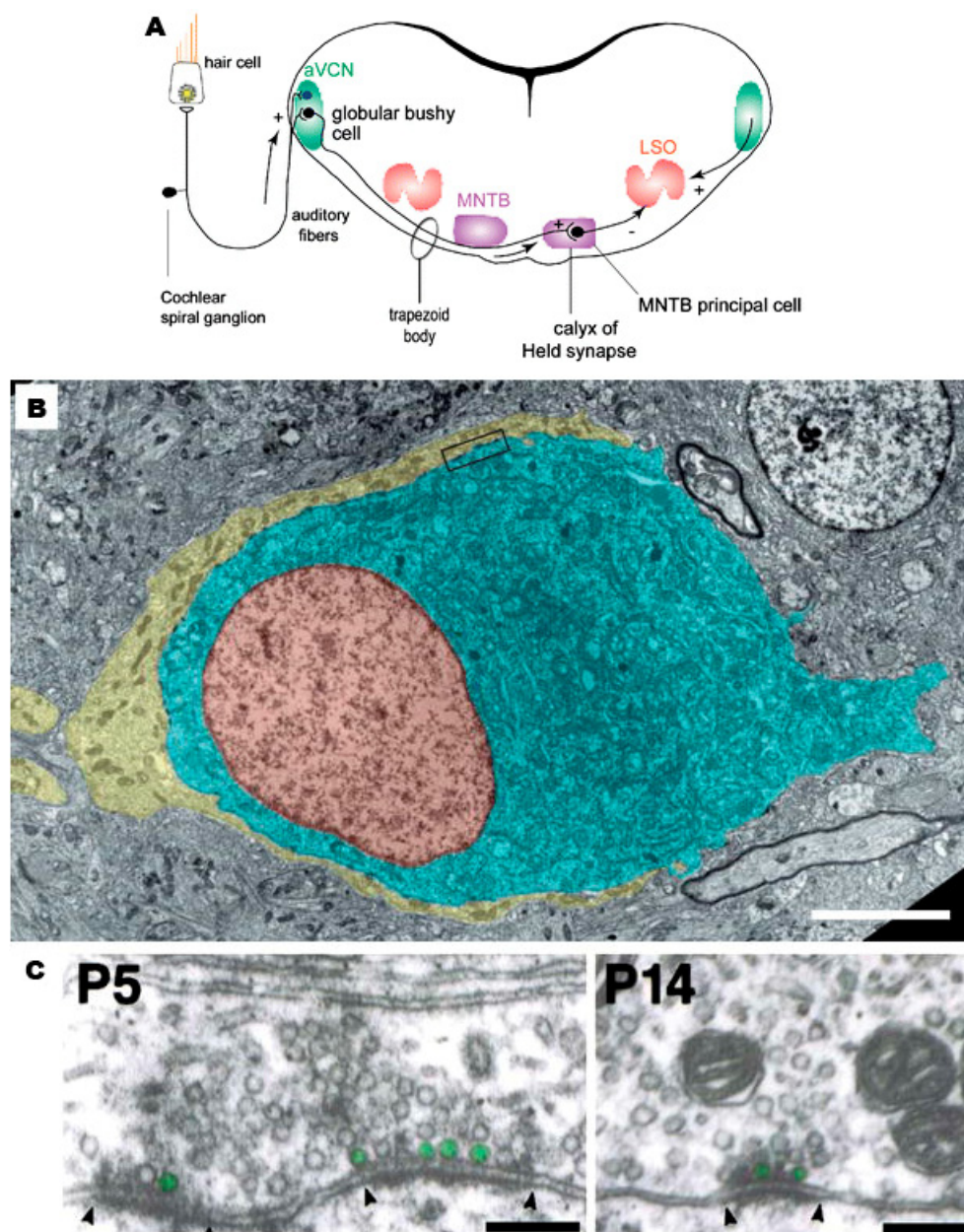
Since most the synapses in the mammalian CNS with a pivotal role in

information processing are fast glutamatergic connections, the setup of a new preparation at which direct presynaptic patch-clamp recordings were possible and at which glutamate was the neurotransmitter was desirable (Schneppenburger and Forsythe, 2006). Moreover, it was of great advantage to find a synapse where it was possible to alter experimentally the composition of the pre- and postsynaptic cytoplasm, allowing testing of the effects of pharmacological compounds on neurotransmission (von Gersdorff and Borst, 2002).

More than ten years ago, an important step toward unraveling synaptic function and plasticity in great detail was the simultaneous patch-clamp recording from a glutamatergic giant presynaptic terminal, the so-called calyx of Held, and its principal neuron in the medial nucleus of the trapezoid body (MNTB; (Forsythe, 1994; Borst et al., 1995).

The calyx of Held terminal is thought to arise from globular bushy cells in the anterior ventral cochlear nucleus (aVCN, Fig.2; (Friauf and Ostwald, 1988; Spirou et al., 1990; Kuwabara et al., 1991; Smith et al., 1991). It therefore forms a tertiary synapse in the auditory pathway. The MNTB principal cells provide inhibitory projections to neighboring nuclei in the superior olivary complex (SOC), including the lateral superior olive (LSO, Fig. 2; (Tollin, 2003) and the medial superior olive (MSO; (Banks and Smith, 1992; Joris et al., 1998; Brand et al., 2002). The LSO and MSO are the first nuclei in which binaural information converges. Therefore, the calyx of Held-MNTB synapse forms a fast *inverting* relay, at which excitation originating from the contralateral cochlea is converted into inhibition to the ipsilateral auditory brainstem. This circuitry presumably leads to intensity comparison of sound arriving at either ear. The differences in sound intensity from each cochlea can be used to locate the

sound source in space (Oertel, 1999; Trussell, 1999). For this task, the calyx of Held has developed to a highly reliable synapse, assuring that every AP arriving at the presynaptic terminal will lead to a postsynaptic AP with a high probability (Taschenberger and von Gersdorff, 2000), thus phase-locking the acoustic signal.



One striking feature of this synapse is that most presynaptic terminals contact only one postsynaptic cell. Moreover, it receives no other substantial synaptic input (Fig. 2B) (Forsythe, 1994); therefore synaptic integration at this synapse does not play a significant role.

Using presynaptic patch-clamp recordings at the calyx of Held, it was possible, for the first time, to measure transmitter release under defined intracellular ionic and membrane potential conditions. This technical achievement was then combined with optical, pharmacological and molecular techniques that have been easily applied at this synapse, to unveil the properties of synaptic transmission. For instance, measurements of the amplitude and time course of AP-evoked Ca^{2+} influx (Borst and Sakmann, 1996, 1998a), the sensitivity of the putative Ca^{2+} sensor (Bollmann et al., 2000; Schneggenburger and Neher, 2000), and the endogenous Ca^{2+} buffer equilibration and extrusion rates of intracellular Ca^{2+} (Helmchen et al., 1997) were accurately made.

◀ **Figure 2. The calyx of Held synapse in the auditory brainstem circuit**

A, Representation in the coronal plane of the brainstem auditory pathway and the calyx of Held synapse, which forms part of the auditory circuit at the level of the superior olivary complex (SOC). Bushy cells in the anterior ventral cochlear nucleus (aVCN) receive excitatory input from the auditory nerve fibers. The calyx of Held arises from globular bushy cells in the aVCN onto a principal cell in the medial nucleus of the trapezoid body (MNTB). The principal cells provide an inhibitory projection to other nuclei of the SOC such as the lateral superior olive (LSO). The calyx of Held is thus a tertiary auditory synapse that rapidly relays afferent activity, providing the LSO and other nuclei with (inhibitory) information with regard to sound arriving at the contralateral ear. Taken from Schneggenburger and Forsythe (2006) **B**, Electron micrograph of the calyx of Held from a P9 rat (*yellow* presynaptic calyx, *blue* postsynaptic MNTB principal neuron, *red* its nucleus, *boxed area* active zone). *Bar* 5 μm . Taken from Sätzler et al. (2002). **C**, Electron micrograph images of active zones within calyces of Held (*green* vesicles identified as morphologically docked). *Left*, two neighboring active zones from a P5 rat. *Right*, single active zone in a P14 rat. *Bars* 200 nm. P5 PSDs tend to be larger than a P14 (limits marked by arrow heads). Taken from Taschenberger et al. (2002).

Furthermore, the latency, size and kinetics of the spontaneous and evoked excitatory postsynaptic currents (EPSCs; (Borst and Sakmann, 1996; Sahara and Takahashi, 2001)) were precisely studied. And recently, Wimmer et al. (2004) opened a new line of molecular structure-function studies in mammalian central synapses by using stereotaxic delivery of viral gene vectors into presynaptic terminals of the calyx of Held synapse.

While most of these studies focused on the detailed mechanisms involved in exocytosis and modulation of transmitter release, other publications investigated how synaptic transmission is refined during the maturation of rat and mouse synapses. Here, synaptic properties were compared before and after the onset of hearing (P12-13). These studies reported that, during postnatal development, morphological and functional synaptic changes eventually transform this synapse into a fast and reliable relay (Taschenberger and von Gersdorff, 2000; Futai et al., 2001; Iwasaki and Takahashi, 2001; Joshi and Wang, 2002; Taschenberger et al., 2002). The next section introduces these developmental modifications at the calyx of Held synapse.

1.4 Developmental maturation at the calyx of Held synapse

1.4.1 Presynaptic changes

During early postnatal development, the calyceal terminal undergoes striking morphological changes (Kandler and Friauf, 1993). Before P12, it resembles a cup-shaped structure covering about 40% of the postsynaptic cell surface (Fig. 2B) (Kandler and Friauf, 1993; Sätzler et al., 2002; Hoffpauir et al., 2006), but already at P14 it changes to a finger-like fenestrated structure (Morest, 1968;

Rowland et al., 2000; Wimmer et al., 2006). Moreover, larger postsynaptic densities (PSDs) breakup into smaller PSDs during development (Fig. 2C), leading to a decrease in the size but an increase in the number of active zones (AZs) in adults. These morphological changes support the idea that glutamate is cleared more efficiently from the synaptic cleft (fenestrated structure) (Taschenberger et al., 2002) and a rapid local endocytosis can occur (more space for the endocytotic machinery in the periphery of small AZs) (Roos and Kelly, 1999; Teng and Wilkinson, 2000).

In addition, by selectively manipulating protein composition in the calyx terminal in vivo, Wimmer et al. (2006) have recently described so-called donut-like assemblies composed of clusters of up to 800 synaptic vesicles, six to nine mitochondria, and five to nine AZs. Interestingly, donut-like assemblies only appear during the maturation of the calyx of Held after the opening of the auditory canal (P11-12). This arrangement of the release machinery (vesicle clusters and AZs) together with mitochondria may be optimal for a fast re-supply of ATP and for local sequestration of Ca^{2+} into mitochondria (Billups and Forsythe, 2002).

Functional presynaptic changes include a shortening of the AP waveform and a decrease of synaptic delays during development (Taschenberger and von Gersdorff, 2000). A shortening in AP waveform, could lower release probability, as Ca^{2+} channels close more rapidly; this would avoid early depletion of vesicles leading to a reduction in the level of short-term depression in mature synapses. Shorter delays and a more synchronous release of glutamate may lead to a better preservation of the timing of auditory signals. A developmental increase in the amplitude of presynaptic Ca^{2+} currents was also observed

(Chuhma and Ohmori, 1998; Taschenberger et al., 2002), together with a switch in the Ca^{2+} channel subtypes expressed by the calyx. At P8-10, they are a mixture of R, N and P/Q Ca^{2+} channels (Wu et al., 1999), whereas from P12 they are mostly of the P/Q subtype (Iwasaki and Takahashi, 1998).

1.4.2 Postsynaptic changes

The kinetics of AMPA receptor-mediated EPSCs become significantly faster at P14 MNTB principal cells. The fast decay time constant of AMPA EPSCs is caused by the fast rates of AMPA-receptor deactivation and desensitization (Schneppenburger and Forsythe, 2006). These fast rates are probably determined by the high expression levels of the AMPA-receptor *flop* splice variant in these neurons, as revealed by single-cell polymerase chain reaction (Geiger et al., 1995; Koike-Tani et al., 2005). Fast AMPA-receptor signalling is seen as an adaptation for the preservation of timing information in auditory circuits (Trussell, 1999).

AMPA EPSCs from rats exhibit little change in their mean peak amplitudes during development (Taschenberger and von Gersdorff, 2000; Iwasaki and Takahashi, 2001). However, studies in mice, suggest a 3-fold increase in AMPA EPSCs amplitude at P14 compared to P8 (Futai et al., 2001; Joshi and Wang, 2002). The increase of AMPA EPSCs amplitude in mice could be attributed to an increase in the number and/or clustering of AMPA receptors, elevated vesicle release probability and/or a higher vesicle pool size in mature animals. Since release probability decreases during development, a bigger pool size is probably the underlying cause of larger AMPA EPSCs, although a small

increase in quantal size is also observed in older mice (as measured from spontaneous miniature EPSCs) (Yamashita et al., 2003).

Furthermore, a strong developmental decrease in NMDA receptor-mediated EPSCs has been observed both for mice and rat (Taschenberger and von Gersdorff, 2000; Futai et al., 2001; Iwasaki and Takahashi, 2001; Joshi and Wang, 2002), with only a small NMDA EPSC remaining after P20. After the onset of hearing (P12-13), NMDA amplitudes decrease 5 to 6-fold the amplitudes at P8. Interestingly, ablation of the cochlea in P7 mice prevents downregulation of NMDA receptor expression in adults, suggesting that these changes are driven by auditory activity-dependent processes (Futai et al., 2001).

The decay time constants for NMDA EPSCs decrease during development from about 80 ms to 50 ms (Joshi and Wang, 2002), consistent with a switch from the slower gating NR2B subunit to the faster gating NR2A NMDA subunit (Futai et al., 2001). However, experiments using the drug ifenprodil, a specific blocker of the NR2B subunit (Williams, 1993), showed only subtle developmental changes in subunit composition (Joshi and Wang, 2002).

1.4.3 Short-term plasticity

During development, synaptic depression in response to high-frequency stimulation is reduced (Taschenberger and von Gersdorff, 2000; Iwasaki and Takahashi, 2001; Joshi and Wang, 2002; Taschenberger et al., 2005). This change might be due to the fenestrated finger-like structure of the adult calyx terminal, which allows a faster diffusion of glutamate out from the synaptic cleft, thus reducing desensitization of AMPA receptors (Taschenberger et al., 2002;

Taschenberger et al., 2005). Moreover, evidence of a larger readily releasable pool (RRP) (Taschenberger and von Gersdorff, 2000; Iwasaki and Takahashi, 2001) and a lower transmitter release probability in the mature terminal (Taschenberger et al., 2002; Taschenberger et al., 2005), would prevent a rapid depletion of synaptic vesicles when stimulated at high frequencies. Finally, the recovery rate from synaptic depression seems to be stable during development (Iwasaki and Takahashi, 2001; Joshi and Wang, 2002), suggesting constant kinetics of synaptic vesicle replenishment. This finding further supports the idea that the main underlying mechanisms for a reduction in depression are a lower release probability and a larger vesicle pool.

In summary, the calyx of Held-MNTB synapse develops into a robust and highly reliable relay, through profound morphological and functional changes. These modifications take place at the same developmental period for both the presynaptic terminal and the postsynaptic cell. How is this precise refinement in synaptic structures and release machinery achieved? What is the role of sensory activity in shaping this fast glutamatergic auditory synapse after the onset of hearing? Although it is generally assumed that sensory input shapes the strength of synaptic properties in neurons, there is very little *in vivo* evidence on the effects of activity during development. The calyx of Held synapse offers a valuable model to attempt answering these questions.

1.5 Aim of this study

Relatively little is known about the role of presynaptic afferent activity during the above mentioned maturation process (Futai et al., 2001). Synaptic activity in auditory brainstem circuitries is driven before hearing onset by *spontaneous*

(Beutner and Moser, 2001) and after the onset of hearing primarily by *sound-evoked* glutamate release from cochlear hair cells. Transmitter release from cochlear inner hair cells (IHCs) is governed by voltage-gated L-type Ca^{2+} channels of the $\text{Ca}_v1.3$ subtype (Brandt et al., 2003) whereas N and P/Q and not L-type (Iwasaki and Takahashi, 1998) Ca channels control release in higher synapses along the auditory pathways (Iwasaki et al., 2000; Oleskevich and Walmsley, 2002). By comparing functional properties of P14-17 calyx of Held synapses developing in the absence of *spontaneous* as well as *sound-evoked* cochlea-driven afferent activity in *Ca_v1.3 subunit-deficient* ($\text{Ca}_v1.3^{-/-}$) mice (Platzer et al., 2000) with those developing in wildtype (*wt*) mice we are able to determine if previously described developmental changes in the functional properties of this synapse arise from intrinsic maturation processes or whether they are driven by afferent nerve activity.

2 MATERIALS AND METHODS

2.1 Slice preparation

The experimental approach to record from acute brain slices is based on a procedure described before by Borst et al. (1995). $Ca_v1.3^{-/-}$ (Platzer et al., 2000) or *wt* mice (C57BL/6) were killed by decapitation and brainstem slices were obtained from postnatal day (P) 8-17 animals. Having removed the cranial calotte, a transversal cut with the scalpel separated the caudal part of the cerebrum from its rostral part including the optic lobes. For an advantageous orientation of the tissue during slicing, the remaining cerebrum was cut at an angle of about 20° to the midsagittal plane (Fig. 3, thick grey line). After cutting the lateral ventral nerves with the scalpel, the caudal part of the brain was detached from the rest of the head. The isolated tissue thus included the caudal cerebrum, the cerebellum, and the brainstem. For smoother cutting of slices, the pia mater and arachnoidea were removed from the ventral surface of the brainstem with forceps without damaging the tissue below.

Then, the brainstem was quickly immersed in ice-cold low Ca^{2+} artificial cerebral spinal fluid (aCSF) containing (in mM): NaCl (125), KCl (2.5), $MgCl_2$ (3), $CaCl_2$ (0.1), glucose (25), $NaHCO_3$ (25), NaH_2PO_4 (1.25), ascorbic acid (0.4), myo-inositol (3), Na-pyruvate (2), pH = 7.3 when bubbled with carbogen (95% O_2 , 5% CO_2). The low temperature and a low extracellular Ca^{2+} concentration $[Ca^{2+}]_e$ (0.1 mM) was chosen to decrease metabolic processes, and to avoid hypoxic damage of the nerve cells.

The brainstem was glued (UHU Sekundenkleber, UHU, Germany or similar) onto the stage of a VT1000S vibratome (Leica, Germany). On the ventral surface of the brainstem, the brighter area of the trapezoid body served as a

shaped platinum wire. The slice was continuously perfused with a flow rate of about 1 ml/min, and the extracellular aCSF solution could be changed according to the experimental design. A complete exchange of the extracellular solution was accomplished within one to two minutes.

2.2 Electrophysiology

Whole-cell patch-clamp recordings were made from calyx of Held terminals and MNTB principal neurons using an EPC-10 amplifier (HEKA, Germany). Analog signals were digitized and stored on disk using 'Pulse 8.77' software (Heka, Germany) running on a Dell Optiplex GX260 PC (1.8 GHz, 256 MB RAM; Dell). Sampling intervals and filter settings were $\leq 20 \mu\text{s}$ and 4.5 kHz, respectively.

The two headstages containing the preamplifiers were mounted on motorized micromanipulators MP-285 (Sutter Instrument Company, Novato, CA, USA), and the coupled pipette holders were airtight connected to air pressure sensors, and a mouthpiece for oral pressure adjustment. Ag/AgCl electrodes connected the preamplifiers with the intracellular solution in the patch pipette, and via a bath electrode with the extracellular solution.

MNTB cells and calyces of Held were visualized by infrared illumination IR-DIC microscopy through a 40x water-immersion objective (NA = 0.8) using an upright BX51WI microscope (Olympus, Germany) equipped with a 1.5-2x pre-magnification and a VX45 CCD camera (PCO, Germany).

Slight pressure was applied to the pipette when approaching the cell, being softer for presynaptic recordings. After contact with the plasma membrane, releasing the pressure together with an abrupt change to slightly negative values, led to a tight and stable seal reaching a resistance of several G Ω . Having obtained a G Ω seal, short suction pulses ruptured an opening into the

cell membrane underneath the tip of the patch pipette. The achieved series resistance was about two times larger than the pipette resistance alone (Sakmann and Neher, 1995). All experiments were carried out at room temperature.

Patch pipettes were pulled from soft glass (1.65 mm diameter, 0.55 mm wall thickness; WPI, Sarasota, FL, USA) on a vertical two-step PIP-5 pipette puller (Heka, Germany). To reduce stray capacitance and to slow down capacitive transients for easier software capacitance compensation, pipettes were coated with dental wax. Open tip resistance was 1.5-3 M Ω for postsynaptic and 3.5-5 M Ω for presynaptic recordings. Access resistance (R_s) was ≤ 20 M Ω for presynaptic and ≤ 10 M Ω for postsynaptic recordings.

To compensate for charging transients of the pipette wall, and of the cell membrane, both were corrected for by using the internal, software controlled compensation circuits of the EPC-10 amplifier. In the cell-attached configuration, the pipette capacitance and series resistance could nicely be compensated, and in the whole-cell mode the cell membrane capacitance and membrane resistance were compensated, too. To correct for membrane voltage errors due to high access resistances to the cell, the automatic EPC-10 R_s compensation has been used (time constant of 2-10 μ s). R_s was routinely compensated 50% during presynaptic and 75-95% during postsynaptic voltage-clamp experiments.

For measuring presynaptic Ca^{2+} currents ($I_{Ca(V)}$) and membrane capacitance (ΔC_m), pipettes were filled with a solution containing (in mM): Cs-gluconate (130), TEA-Cl (30), HEPES (10), BAPTA (0.05), Na_2 -phosphocreatine (5), ATP-Mg (4), GTP (0.3), pH=7.3 with CsOH. The bath solution was supplemented with 1 μ M TTX, 40 mM TEA-Cl and 100 μ M 4-AP to suppress voltage activated

sodium and potassium currents. ΔC_m was measured using a software lock-in amplifier (HEKA Pulse 8.77) by adding a 1 kHz sine wave voltage command (amplitude ± 35 mV) to the holding potential (V_h) of -80 mV. ΔC_m was obtained from the averaged C_m value during a 50 ms time window ≥ 190 ms after the end of the depolarizations. Terminals with a leak current > 120 pA or slowly decaying tail currents following $I_{Ca(V)}$ were discarded from the analysis.

Presynaptic calyceal action potentials (APs) were elicited by afferent fiber stimulation via a bipolar stimulation electrode placed half way between the brainstem midline and the MNTB (for reference see Fig. 2). Stimulation pulses (100 μ s duration) were applied using a stimulus isolator unit (AMPI, Israel), with the output voltage set to 1-2 V above threshold (≤ 35 V). APs were measured in the current-clamp mode of the EPC-10 after adjusting the fast-capacitance cancellation while in cell-attached mode. For measuring calyceal APs, pipette were filled with a solution consisting of (in mM): K-gluconate (85), KCl (85), HEPES (10), EGTA (5), Na₂-phosphocreatine (10), ATP-Mg (4), GTP (0.3), pH=7.3 with KOH.

Excitatory postsynaptic currents (EPSCs) were measured using pipette solution consisting of (in mM): CsCl (150), TEA-Cl (10), HEPES (10), EGTA (5), ATP-Mg (4), GTP (0.3), pH=7.3 with CsOH. For each AP-evoked EPSC (eEPSC) the series resistance (R_s) value was updated and stored with the data using the automated R_s compensation routine implemented in 'Pulse'. Residual R_s errors were compensated off-line for postsynaptic recordings. NMDA eEPSCs were recorded at $V_h = +40$ mV. In P14-17 mice, the peak amplitudes of AMPA eEPSCs frequently exceeded 20 nA at V_h more negative than -40 mV. Except for analysis of their kinetic properties and determining the release time course, AMPA eEPSCs were therefore routinely recorded at $V_h = -40$ mV to reduce

driving force and completely inactivate voltage-gated Na currents in postsynaptic MNTB neurons. Miniature EPSCs (mEPSCs) were recorded at $V_h = -70$ mV. Bicuculline methiodide (25 μ M), strychnine (2 μ M) were routinely included in the bath solution to block inhibitory synaptic currents. TTX was obtained from Alomone Laboratories (Jerusalem, Israel). Bicuculline, strychnine, NBQX and ifenprodil were from Tocris Cookson. All other salts and chemicals were from Sigma.

2.3 Data analysis

All offline analysis was performed with 'IgorPro 5.0' software (Wavemetrics, USA). Presynaptic AP-evoked Ca^{2+} influx was simulated using a Hodgkin-Huxley (HH) type model essentially as described by Borst and Sakmann (1998a) except that the reversal potential of $I_{Ca(V)}$ was set to +45 mV. Presynaptic AP waveforms measured at P14-17 were used to drive the model. The time course of the average activation parameter m^2 was solved numerically using a fifth-order Runge-Kutta-Fehlberg algorithm implemented in IgorPro.

For analysis of eEPSCs, traces were corrected for remaining series-resistance errors (Neher and Sakaba, 2001b) using the R_s values stored in the data files (assuming a linear IV-relationship with a reversal potential of 0 mV).

Miniature EPSCs (mEPSCs) were detected using a sliding template algorithm (Jonas et al., 1993; Clements and Bekkers, 1997). The mEPSC template length of 4 ms allowed detection of non-overlapping mEPSCs up to a maximum rate of 250 events/s.

The release time course ($r(t)$) was determined by deconvolving eEPSCs with idealized mEPSC waveforms obtained from the same synapses. Deconvolution was carried out in the frequency domain using Discrete Fourier transforms implemented in IgorPro. The Fourier transform of eEPSC ($F\{eEPSC\}$) was divided by that of the quantal response ($F\{mEPSC\}$) and the release rate was obtained from the inverse Fourier transform of this quotient $r(t)=F^{-1}\{F\{eEPSC\}/F\{mEPSC\}\}$ (Van der Kloot, 1988; Diamond and Jahr, 1995; Hefft and Jonas, 2005). Analysis of kinetic properties and deconvolution analysis were restricted to AMPA eEPSC having peak amplitudes ≤ 15 nA at $V_h = -70$ mV to avoid non-linear summation of quanta due to AMPAR saturation. All average data are reported as mean \pm SEM. For statistical tests we assumed that the measured quantities were normally distributed and used an unpaired two-tailed Student's t test. Statistical significance was set at $p < 0.05$.

3 RESULTS

Mice begin to detect sound during the second postnatal week (Mikaelian and Ruben, 1964; Kikuchi and Hilding, 1965). At P10, only a small fraction of mice pups show auditory brainstem responses after click stimulation. This number reaches 100% at around P13 (Futai et al., 2001). Because we wanted to study how spontaneous and sound-evoked afferent nerve activity shapes the maturation process at the calyx of Held, most of our analysis was carried out after the onset of hearing on synapses of P14-17 *wt* mice in comparison to $Ca_v1.3^{-/-}$ mice of the same age. In some cases we compared the functional properties of P14-17 synapses to those obtained before hearing onset (P8-11) (For values, see Table 1 and Table 2 at the end of section 3, Results).

3.1 Synaptic transmission in $Ca_v1.3^{-/-}$ synapses

During afferent fiber stimulation, postsynaptic cells of the MNTB typically respond with fast and large action potential (AP) waveforms (Forsythe and Barnes-Davies, 1993a) which are mainly determined by voltage-gated Na^+ (Ming and Wang, 2003; Leao et al., 2005) and K^+ conductances (Forsythe and Barnes-Davies, 1993b; Brew and Forsythe, 1995).

We observed characteristic AP firing at $Ca_v1.3^{-/-}$ MNTB neurons stimulated at 20 Hz trains in current-clamp whole cell recordings (Fig. 4A). At higher time resolution, it is seen that late APs in the train activate slower and exhibit more jitter (Fig. 4A right), suggesting that excitatory postsynaptic potentials (EPSPs) need more time to reach threshold. These typical depressed EPSPs are probably due to depression in later EPSCs during the train (Chuhma and

Ohmori, 1998; Taschenberger and von Gersdorff, 2000; Brenowitz and Trussell, 2001).

In whole cell voltage-clamp recordings, during single stimulus application, principal cells of the MNTB exhibit fast and slowly activated excitatory postsynaptic currents (EPSCs). These fast and slow EPSCs are mediated by two types of ligand-gated ion channels, AMPA and NMDA receptors, respectively (Forsythe and Barnes-Davies, 1993a).

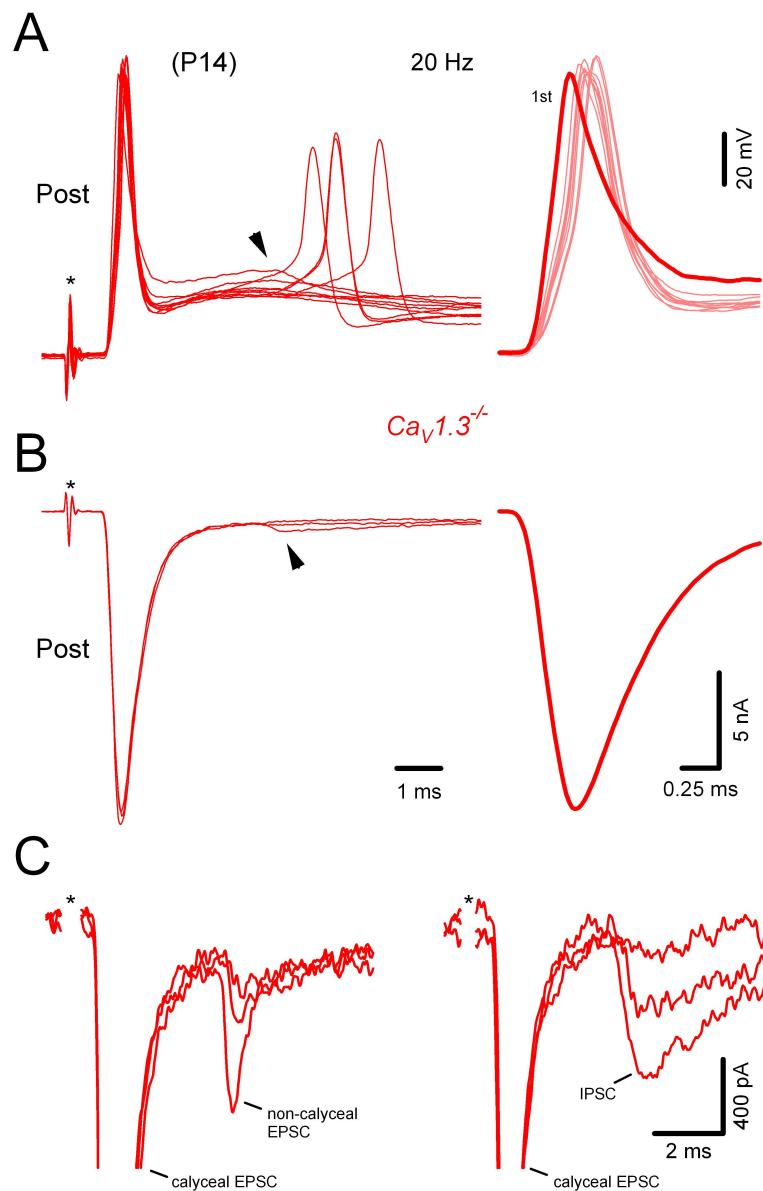


Fig. 4B shows characteristic EPSCs elicited after a single stimulus (100 μ s) using afferent fiber stimulation. In a few recordings, after calyceal EPSCs, we observed smaller EPSCs or inhibitory PSCs (IPSCs) with a delayed onset of activation (Fig. 4B, arrow and 4C). Small EPSCs with fast kinetics (Fig. 4C, left panel) probably correspond to small EPSPs recorded in current-clamp whole cell configuration also around 4 ms after stimulation (Fig. 4A, arrow). Presumably, these small EPSPs may trigger the observed slower and smaller APs in postsynaptic cells (Hamann et al., 2003).

A subset of recordings exhibit slower activated and decaying currents (Fig. 4C, right panel). They present typical kinetics of activation and deactivation previously reported for IPSCs, which are much slower in comparison to EPSCs kinetics (Forsythe and Barnes-Davies, 1993a). Altogether, these results demonstrate that the basic mechanism of synaptic transmission is intact in $Ca_v1.3^{-/-}$ synapses.

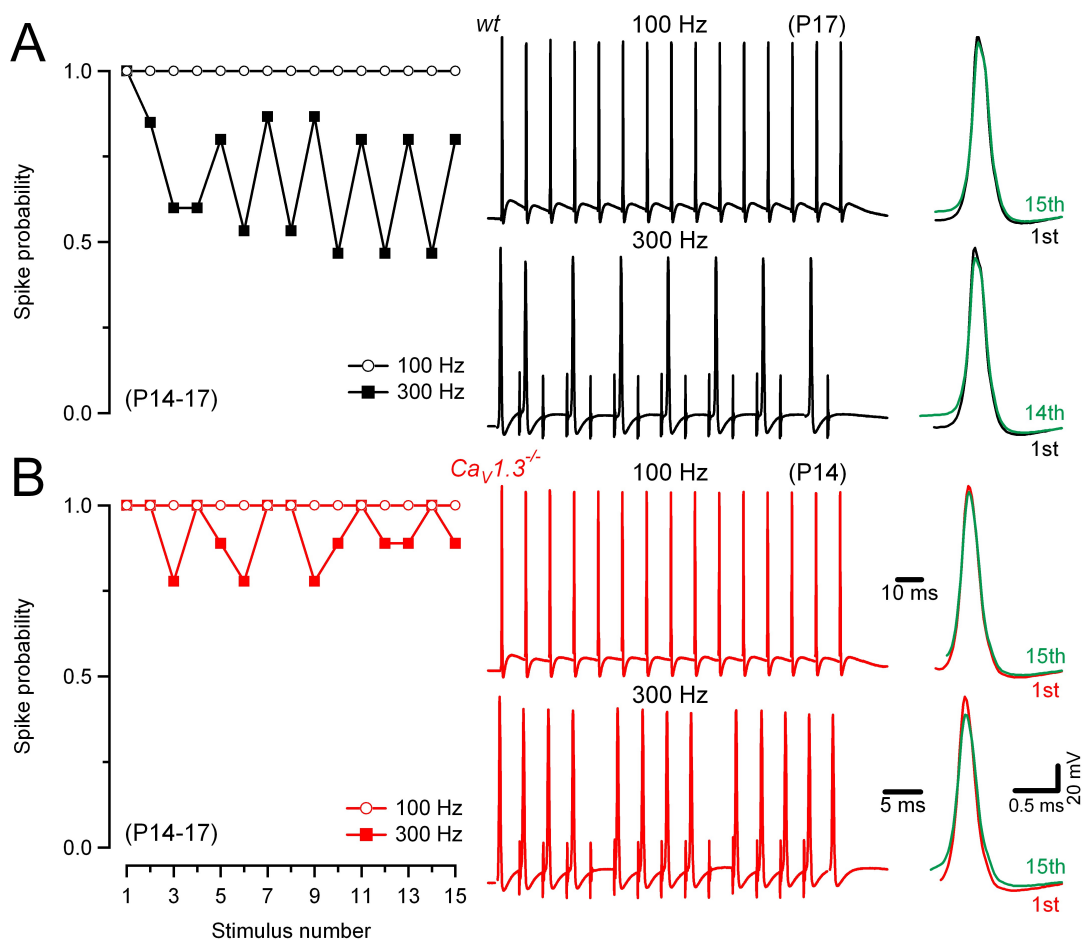
◀ **Figure 4. Synaptic transmission in mature $Ca_v1.3^{-/-}$ mice**

A, Postsynaptic APs recorded in current-clamp whole cell configuration from a P14 MNTB neuron in a $Ca_v1.3^{-/-}$ mouse (Resting membrane potential (V_r) \sim -70 mV). *Left panel*, 10 responses to a train of afferent stimuli (20 Hz) are superimposed. In some recordings, we observed a small delayed EPSP (\sim 4 ms) (arrow), which occasionally was suprathreshold and triggered another AP. *Right panel*, expanded view of the same 10 APs as in left panel. Note that late responses during the train exhibit jitter. **B**, *Left panel* shows voltage-clamp whole cell recordings of 3 sample EPSCs from the same neuron as in **A** (V_h = -40 mV). Note the small delayed PSC (arrow). *Right panel*, expanded time scale of one EPSC as in the left panel. Both current-clamp (**A**) and voltage clamp (**B**) recordings were aligned at stimulus artifacts (*) to compare the timing of APs and synaptic delays of EPSCs as well as small EPSPs and small input currents. Time scales are the same for **A** and **B**. Current and voltage scales are the same for left and right in **A** and **B**, respectively. **C**, Sample traces illustrating delayed non-calyceal EPSCs and inhibitory PSCs (IPSCs) (*left and right panel*, respectively) (V_h = -40 mV). Note the slower kinetics of IPSCs compared to EPSCs. Equilibrium potential of Cl^- , V_{Cl} = -11.37 mV. Stimulus artifacts were blanked for clarity. All experiments illustrated in this and subsequent figures were carried out at room temperature.

3.2 Presynaptic action potentials of $Ca_v1.3^{-/-}$ mice during trains

After the onset of hearing (P12-13), as a result of diverse pre- and postsynaptic changes, the fidelity of high-frequency synaptic transmission at the calyx of Held-MNTB synapse is developed. (Taschenberger and von Gersdorff, 2000; Joshi and Wang, 2002; Taschenberger et al., 2002).

To examine the behaviour of the calyx of Held presynaptic terminal under physiological conditions, we recorded presynaptic APs in response to trains of high frequency stimuli (100 Hz and 300 Hz, 15 stimuli). We found that both *wt* and $Ca_v1.3^{-/-}$ calyces were capable of responding to 100 Hz stimulation, but multiple failures were observed in both synapses at the higher frequency tested (300 Hz) (Fig. 5, middle panel).



For P14-17 synapses, spike probability was slightly lower in *wt* than in *Ca_v1.3^{-/-}* mice (Fig 5A and 5B), but the difference was not significant, apparently because of the small number of train repetitions (3) and of neurons analyzed (5 and 3 for *wt* and *Ca_v1.3^{-/-}*, respectively).

Previous studies in the rat calyx of Held (P8-10) indicated AP broadening during prolonged trains (Borst and Sakmann, 1999). We therefore asked if a distinct broadening (if any) of presynaptic APs occurs when calyces of P14-17 *wt* and *Ca_v1.3^{-/-}* mice are stimulated using trains of 15 stimuli at frequencies of 100 Hz and 300 Hz .

Fig. 5A and 5B, right panel, show first (1st) and last (14th or 15th) AP waveforms superimposed at an expanded time scale. As previously reported (Taschenberger et al., 2002), during short trains only a minor broadening of APs was detected with no apparent differences between *wt* and *Ca_v1.3^{-/-}* mice.

◀ **Figure 5. Presynaptic AP failure occurrence is similar between *wt* and *Ca_v1.3^{-/-}* mice**

A, *Middle*, trains of 15 stimuli evoked by afferent fiber stimulation and delivered at 100 Hz (upper panel) and 300 Hz (lower panel) to a P17 *wt* (*black*) synapse. *Right*, first and last APs in the train are superimposed at higher time resolution. *Left*, in P14-17 *wt* (*black*) synapses, probabilities of action potential firing during stimulus trains at 100 Hz (*open circles*, n = 6) and 300 Hz (*black squares*, n = 5) were measured as the fraction of APs fired for each stimulus during 3 repetitions delivered at 15 sec intervals. **B**, Same as in **A** for P14-17 *Ca_v1.3^{-/-}* (*red*) presynaptic terminals. Sample traces in the middle panel were recorded from a P14 *Ca_v1.3^{-/-}* calyx of Held. Spike probability was calculated from 4 and 3 cells of *Ca_v1.3^{-/-}* mice at 100 Hz and 300 Hz, respectively. In both *wt* (*black*) and *Ca_v1.3^{-/-}* (*red*) mice, AP halfwidths were stable throughout the train (*right panel*); however, amplitudes of APs were slightly diminished at 100 Hz stimulation and even more at 300 Hz. At the highest frequency tested (300 Hz), action potential failures occurrence was higher than at 100 Hz (*middle panel*), thus diminishing the probability of AP firing similarly in *wt* (*black*) and *Ca_v1.3^{-/-}* (*red*) calyces (*left panel*). V_r was typically around -80 mV in this and subsequent figures for presynaptic AP current-clamp recordings.

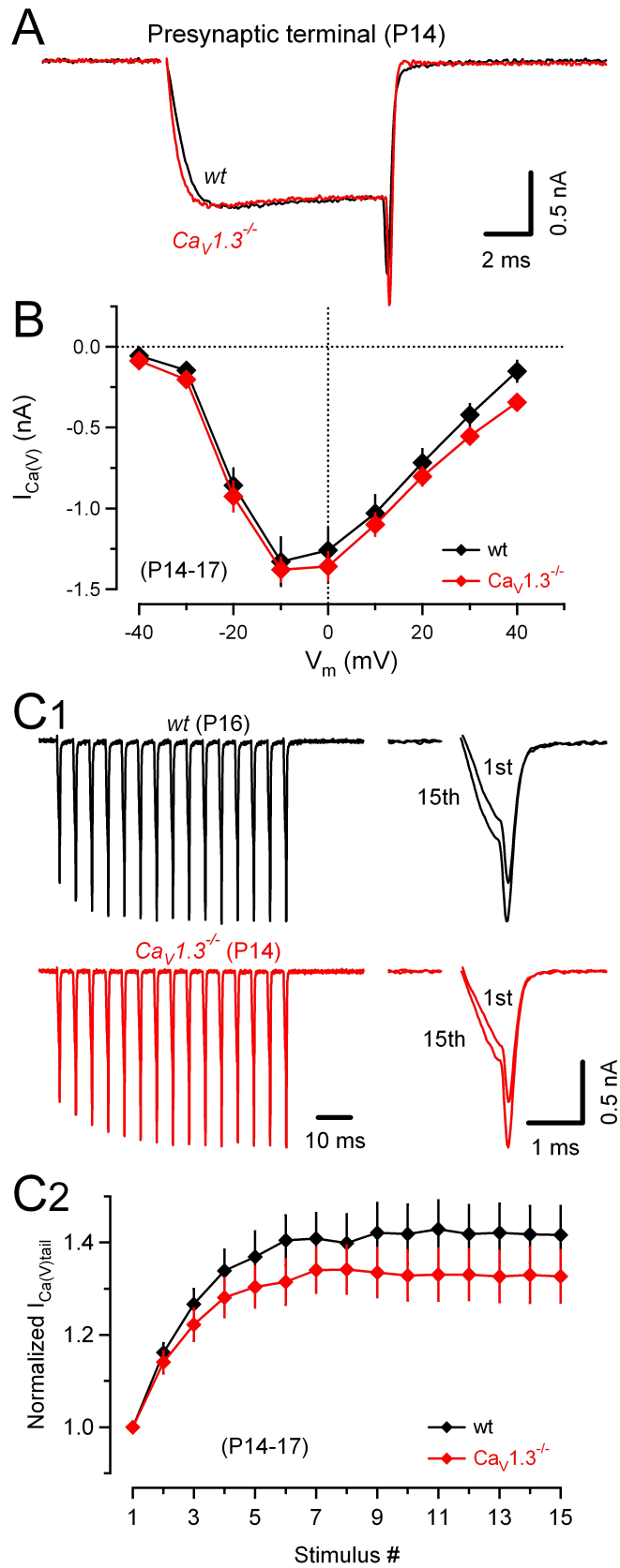
Nevertheless, when AP waveforms were further analyzed, we did observe a small decrease of the 15th compared to the 1st AP amplitude, and this reduction was accentuated when axons were stimulated using 300 Hz trains. However, no differences between *wt* and *Ca_v1.3^{-/-}* calyces were noticed. Thus, we suggest that the capability to follow high frequency inputs is similar in *Ca_v1.3^{-/-}* presynaptic terminals compared to *wt* calyces.

3.3 Presynaptic Ca²⁺ currents and exocytosis in calyceal terminals from *Ca_v1.3^{-/-}* mice

Immature calyces of Held express a mixture of agatoxin-IVA-sensitive P/Q type and conotoxin-GVIA-sensitive N-type Ca²⁺ currents (*I_{Ca(V)}*). The latter component is developmentally down regulated such that after P13, *I_{Ca(V)}* is completely blocked by agatoxin-IVA (Iwasaki et al., 2000).

► **Figure 6. Similar amplitudes and dynamic properties of voltage-gated Ca²⁺ currents in calyceal terminals of *wt* and *Ca_v1.3^{-/-}* mice**

A, Presynaptic *I_{Ca(V)}* recorded in calyx of Held terminals of *wt* (black) and *Ca_v1.3^{-/-}* (red) mice. Calyx terminals were identified by a change in membrane capacitance in response to short depolarizations indicating intact vesicle exocytosis. Terminals were voltage-clamped ($V_h = -80$ mV) and depolarized to 0 mV for 10 ms. Capacitive transients were subtracted on-line using a P/5 protocol. Small transients remaining after online subtraction were blanked for clarity. Pipettes were filled with Cs-gluconate-based solution (50 μ M BAPTA). Voltage-gated Na⁺ and K⁺ conductances were blocked by including 1 μ M TTX, 40 mM TEA and 100 μ M 4-AP in the bath solution. **B**, Current-voltage relationship of presynaptic *I_{Ca(V)}* in calyx of Held terminals of *wt* (black, $n = 8$) and *Ca_v1.3^{-/-}* (red, $n = 7$) mice. Peak *I_{Ca(V)}* was measured during depolarizations (10 ms) from V_h to -40 ... +40 mV. Average amplitudes of *I_{Ca(V)}* and its voltage-dependence were virtually indistinguishable suggesting that the *Ca_v1.3* subunit is absent from calyces of *wt* mice. **C**, Facilitation of *I_{Ca(V)}* during trains of AP-like depolarizations. **C1**, *I_{Ca(V)}* trains of 15 step depolarizations (1 ms, 0 mV, 200 Hz) recorded in terminals of *wt* (black) and *Ca_v1.3^{-/-}* (red) mice (left panel). For comparison, first and last *I_{Ca(V)}* are shown superimposed (right panel). **C2**, Average time course and amplitude of facilitation were similar in *wt* (black, $n = 8$) and *Ca_v1.3^{-/-}* (red, $n = 9$) mice. Error bars represent SEM in this and subsequent figures.

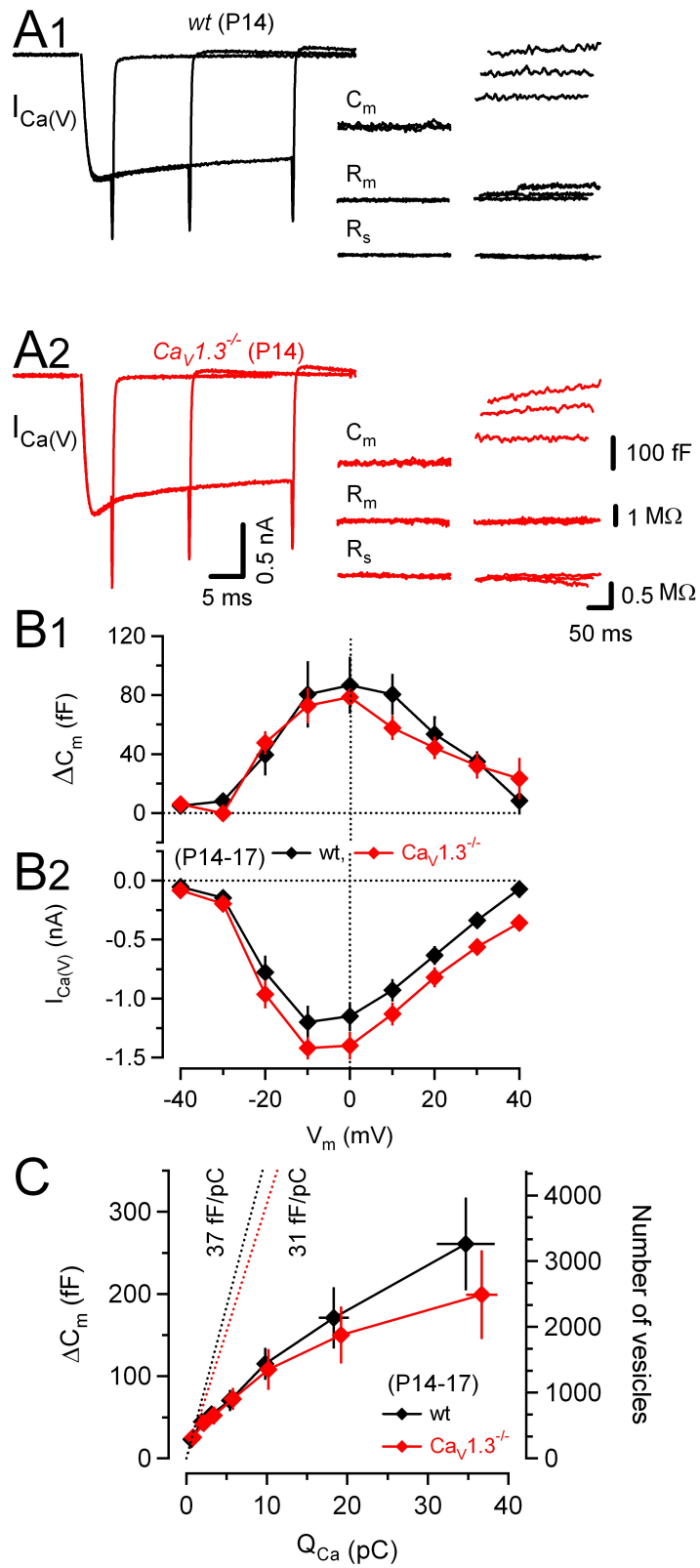


As expected from this pharmacological profile, we found that neither amplitudes nor kinetic properties were different between $I_{Ca(V)}$ recorded in P14-17 terminals of $Ca_v1.3^{-/-}$ mice and that of *wt* mice (Fig. 6A). When measured during 10 ms depolarizations, peak amplitudes of $I_{Ca(V)}$ varied between 0.81 nA and 2.05 nA among different terminals (for average amplitudes see Table 1). $I_{Ca(V)}$ started to activate at a membrane potential of around -30 mV. Its current-voltage relationship was indistinguishable between $Ca_v1.3^{-/-}$ and *wt* mice (Fig. 6B) and similar to that described for P8-10 rat calyces (Borst and Sakmann, 1998a).

A characteristic signature of calyceal $I_{Ca(V)}$ is its frequency-dependent facilitation when elicited repetitively using short AP-like depolarizations (Borst and Sakmann, 1998b; Cuttle et al., 1998). This facilitation is mainly supported by calcium channels of the P/Q type as it is absent from $Ca_v2.1$ -subunit deficient mice (Inchauspe et al., 2004; Ishikawa et al., 2005). We measured activity-dependent facilitation of $I_{Ca(V)}$ using 200 Hz trains of 1 ms step depolarizations (0 mV).

► **Figure 7. Similar kinetics and Ca^{2+} dependence of glutamate release in calyceal terminals of *wt* and $Ca_v1.3^{-/-}$ mice**

A, Presynaptic $I_{Ca(V)}$ recorded during depolarizations of 5, 17 and 33 ms duration from $V_h = -80$ mV to 0 mV (left) and corresponding changes in membrane capacitance (C_m , top traces), membrane resistance (R_m , middle traces) and series resistance (R_s , bottom traces) (right). ΔC_m was estimated from averaged C_m values measured during a 50 ms time window ≥ 190 ms after the end of depolarizations. **B**, Average $I_{Ca(V)}$ (**B2**) and corresponding average ΔC_m values (**B1**) plotted against V_m for step depolarizations of 10 ms duration obtained from 6 *wt* (*black*) and 6 $Ca_v1.3^{-/-}$ (*red*) mice. Note the similar voltage-dependence of $I_{Ca(V)}$ and ΔC_m . **C**, Average ΔC_m values plotted against measured Ca^{2+} charge (Q_{Ca}) during presynaptic depolarizations of variable duration (1, 2, 3, 5, 9, 17 and 33 ms). Pooled data from 9 *wt* calyces and 10 terminals from $Ca_v1.3^{-/-}$ mice (P14-17). Dotted lines represent extrapolations using the first $\Delta C_m/Q_{Ca}$ ratio obtained with an AP-like depolarization (1ms, 0mV). For longer stimuli, $\Delta C_m/Q_{Ca}$ decreases presumably because of vesicle depletion.



As illustrated in Fig. 6C, amplitudes of $I_{Ca(V)}$ facilitated during the first 5 to 7 depolarizations and remained stable thereafter. Neither time course nor magnitude of $I_{Ca(V)}$ facilitation were significantly different between $Ca_V1.3^{-/-}$ and *wt* mice. Average values of $I_{Ca(V)}$ facilitation during 200 Hz trains are given in Table 1.

Having established similar properties of $I_{Ca(V)}$, we next compared amplitudes of exocytotic responses and their Ca^{2+} dependence between calyces of $Ca_V1.3^{-/-}$ mice and those of *wt* mice using presynaptic membrane capacitance measurements. To convert ΔC_m values into vesicle numbers we assumed a single vesicle capacitance of 80 aF (Taschenberger et al., 2002; Sakaba, 2006). Figure 7A illustrates changes in C_m , membrane resistance (ΔR_m) and series resistance (ΔR_s) evoked by short depolarizations (0 mV) of 5 to 33 ms duration in two representative terminals. We restricted our analysis to step depolarizations of ≤ 33 ms duration to prevent slowly decaying tail currents upon repolarization which were frequently associated with longer lasting depolarizations and complicated ΔC_m estimates (Yamashita et al., 2005). To ascertain that the measured ΔC_m reflects vesicle exocytosis following presynaptic Ca^{2+} influx, we measured $I_{Ca(V)}$ and the corresponding ΔC_m as a function of membrane potential (V_m) in a subset of calyces. Figure 7B shows that $I_{Ca(V)}$ and ΔC_m exhibited similar voltage dependence. Both peaked at V_m -10 to 0 mV. ΔC_m declined at $V_m > 0$ mV due to smaller $I_{Ca(V)}$ because of the reduced driving force irrespective of a fully activated Ca^{2+} conductance.

Figure 7C shows the relationship between ΔC_m and presynaptic Ca^{2+} influx (Q_{Ca}) obtained by pooling data from P14-17 terminals of $Ca_V1.3^{-/-}$ ($n=10$) and *wt*

(n=9) mice. In both groups, ΔC_m increased similarly with larger Q_{Ca} . For short AP-like depolarizations (1 ms, 0 mV), we obtained ΔC_m values of 23.3 ± 5.6 fF (291 ± 70 vesicles) and 25.5 ± 4.9 fF (319 ± 61 vesicles) for *wt* and *Ca_v1.3^{-/-}* mice, respectively. The corresponding $\Delta C_m/Q_{Ca}$ ratios were 37 fF/pC and 31 fF/pC for *wt* and *Ca_v1.3^{-/-}* mice, respectively (Fig. 7C broken lines), which is close to values reported before for P12-14 rats (46 fF/pC, Taschenberger et al., 2002). For longer depolarizations, ΔC_m values started to saturate presumably due to vesicle depletion. For the longest step depolarizations we measured similar ΔC_m values of 261 ± 56 fF (3269 ± 706 vesicles) and 199 ± 47 fF (2488 ± 589 vesicles) in terminals of *wt* and *Ca_v1.3^{-/-}* mice, respectively.

3.4 Presynaptic AP waveform in *Ca_v1.3^{-/-}* mice

Taken together, the experiments described above suggest that a given presynaptic AP waveform elicits a similar presynaptic Ca^{2+} influx and releases a similar number of vesicles in terminals from *wt* and *Ca_v1.3^{-/-}* mice. However, the time course of calyceal APs is not invariable (Taschenberger and von Gersdorff, 2000). Since the AP waveform is a powerful regulator of presynaptic Ca^{2+} influx and thereby of release probability (Borst and Sakmann, 1999), we tested whether calyceal APs of *Ca_v1.3^{-/-}* mice would differ from those recorded in *wt* terminals. When measured between P14 to P17, the half-width of presynaptic APs ranged from ~ 140 to ~ 260 μ s. In terminals of *Ca_v1.3^{-/-}* mice, AP waveforms tended to be slower and broader (Fig. 8A, Table 1).

The Ca^{2+} influx evoked by a single P14-17 calyceal AP is difficult to quantify using single electrode voltage-clamp (Borst and Sakmann, 1998a). To elucidate the impact of variable AP duration on AP-evoked release we adopted a HH-type

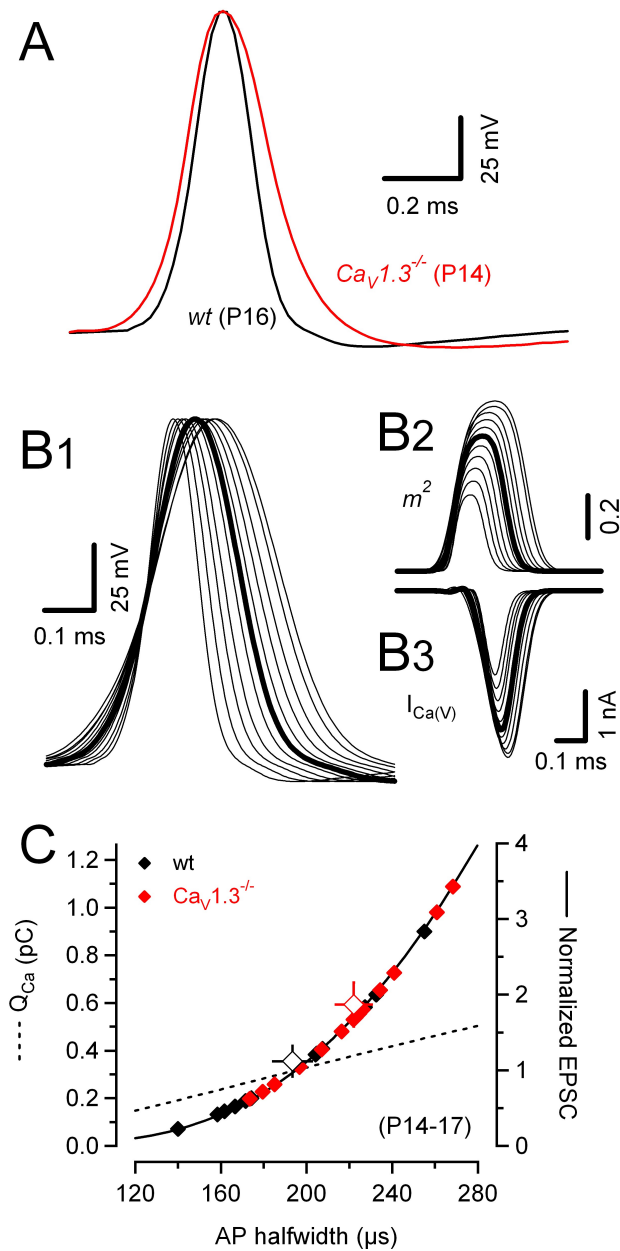
model of $I_{Ca(V)}$ derived by Borst and Sakmann (1998a). The model was driven by the *wt* AP waveform shown in Fig. 8A with its time course slightly compressed or expanded such that the AP half-width ranged from 120 to 280 μ s (Fig. 8B1). The time course of the activation parameter m^2 was then solved numerically (Fig. 8B2) which allowed us to predict presynaptic $I_{Ca(V)}$ (Fig. 8B3) associated with the various AP waveforms.

Figure 8C illustrates that Q_{Ca} depended roughly linearly on AP half-width. To obtain a relationship between AP half-width and relative eEPSC size, we normalized Q_{Ca} to the value obtained with an AP having about average half-width (200 μ s) and raised this quantity to the third power. This takes into account a presumably less steep Ca^{2+} -dependence of release in more mature terminals (Fedchyshyn and Wang, 2005) compared to immature ones (Borst and Sakmann, 1996; Bollmann et al., 2000; Schneggenburger and Neher, 2000).

► **Figure 8. Wider action potentials in calyceal terminals of $Ca_v1.3^{-/-}$ mice**

A, Whole-cell current-clamp recordings of APs evoked by afferent fiber-stimulation in calyces of *wt* (black) and $Ca_v1.3^{-/-}$ (red) mice. Both recordings were obtained after hearing onset. K-gluconate-filled electrodes were used. Resting membrane potential (V_r) was typically around -80 mV. Stimulus artifacts were blanked for clarity. Note the similar amplitude but slower kinetics and longer duration of the calyceal AP in the $Ca_v1.3^{-/-}$ mouse. Calyceal APs recorded in $Ca_v1.3^{-/-}$ mice were on average 15% wider than those recorded in *wt* mice (Table 1). **B**, The *wt* AP shown in (A) was used to drive a HH-type model (Borst and Sakmann, 1998a) to estimate presynaptic Ca^{2+} influx. To simulate variable duration, APs were expanded or compressed in time (**B1**). The time course of the activation parameter m^2 was solved numerically (**B2**) and the corresponding $I_{Ca(V)}$ was calculated (**B3**). Peak m^2 values ranged from 0.36 to 0.81 yielding Q_{Ca} of 0.13 to 0.50 pC. **C**, Dependence of Q_{Ca} and AP half-width and relative EPSC size on AP half-width. Over the range from 120 to 280 μ s, Ca^{2+} influx depended nearly linearly on AP half-width (**C, left axis**). Relative EPSC size was estimated by normalizing the Q_{Ca} to the value obtained with a *wt* AP of average half-width (200 μ s) and raising this quantity to the third power. Measured values of AP half-width were plotted along this function to illustrate the highly nonlinear dependence of EPSC size on AP width and predicting a 1.67 fold larger average eEPSC size for $Ca_v1.3^{-/-}$ mice (**C, right axis**).

When the measured AP half-width values were plotted along this function (Fig. 8C), they predicted relative eEPSC amplitudes which were on average about 67% larger in $Ca_v1.3^{-/-}$ compared with *wt* mice ($p < 0.05$).



3.5 Enhanced synaptic strength in $Ca_v1.3^{-/-}$ mice

Our modeling-based estimates for AP-induced presynaptic Ca^{2+} influx lead us to predict an enhanced release from calyces of $Ca_v1.3^{-/-}$ compared to *wt* mice. We therefore tested synaptic strength by measuring AMPA eEPSCs ($EPSC_{AMPA}$).

Figure 9A shows recordings from synapses of *wt* and $Ca_v1.3^{-/-}$ mice before and after hearing onset. From P8-11 to P14-17, the average weighted decay time constants τ_m decreased similarly in *wt* mice (from 1.50 ± 0.21 to 0.46 ± 0.03 ms) and in $Ca_v1.3^{-/-}$ mice (from 1.33 ± 0.30 to 0.57 ± 0.06 ms) (Fig. 9C) and amplitudes of $EPSC_{AMPA}$ increased (Futai et al., 2001; Joshi and Wang, 2002) (Fig. 9B). The observed increase in $EPSC_{AMPA}$ was, however, much stronger in synapses developing in the absence of cochlea-driven afferent nerve activity (Fig. 9B) such that at P14-17, their average amplitudes were ~ 1.5 times larger in $Ca_v1.3^{-/-}$ compared with *wt* mice ($p < 0.001$; Table 1).

To discriminate between a pre- or postsynaptic locus of the enhanced transmission, we analyzed the variability of AMPA eEPSC amplitudes.

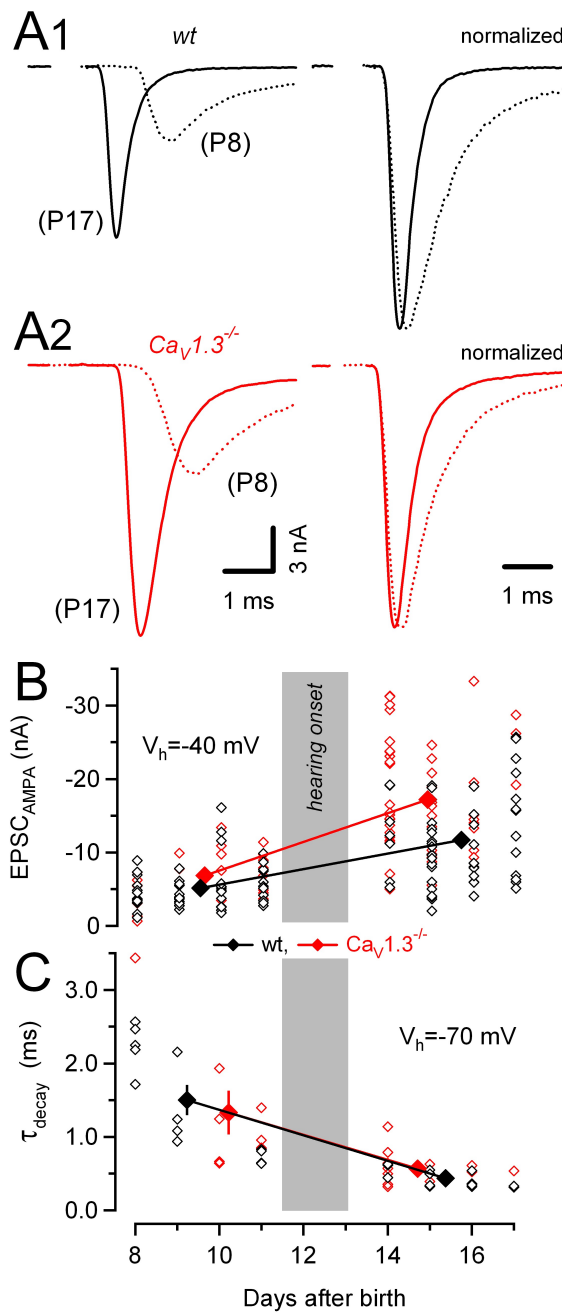
► **Figure 9. Larger AMPA eEPSC peak amplitudes in synapses of $Ca_v1.3^{-/-}$ mice**

A, Representative AMPA receptor-mediated eEPSCs evoked by afferent fiber stimulation in synapses of *wt* (**A1, left**) and $Ca_v1.3^{-/-}$ (**A2, left**) mice ($V_h = -40$ mV). The right panel shows the same traces after normalizing their amplitudes. eEPSCs were aligned at their onsets to facilitate comparison of rise and decay kinetics (Tables 1 and 2). Kinetic properties of eEPSC in synapses of *wt* and those of $Ca_v1.3^{-/-}$ mice were similar. **B**, Scatter plot of AMPA EPSC peak amplitudes vs. age. EPSC peak amplitudes varied over a widespread range at any developmental stage. However, the largest EPSCs were consistently recorded in synapses from $Ca_v1.3^{-/-}$ mice. At P14-17, AMPA EPSCs from $Ca_v1.3^{-/-}$ mice (*red*) were on average 54% larger than those recorded in *wt* mice (*black*). **C**, Scatter plot of the weighted decay time constants of AMPA EPSCs. Developmental acceleration of AMPA EPSC kinetics proceeded similarly in *wt* and $Ca_v1.3^{-/-}$ mice.

For a binomial model of release, the coefficient of variation (CV) depends exclusively on the presynaptic parameters p and N :

$$CV = \frac{\sqrt{Nq^2 p(1-p)}}{Nqp} = \sqrt{\frac{1-p}{Np}}$$

Raising quantal content ($M=N \cdot p$) by increasing N , p or both is thus expected to lower CV.



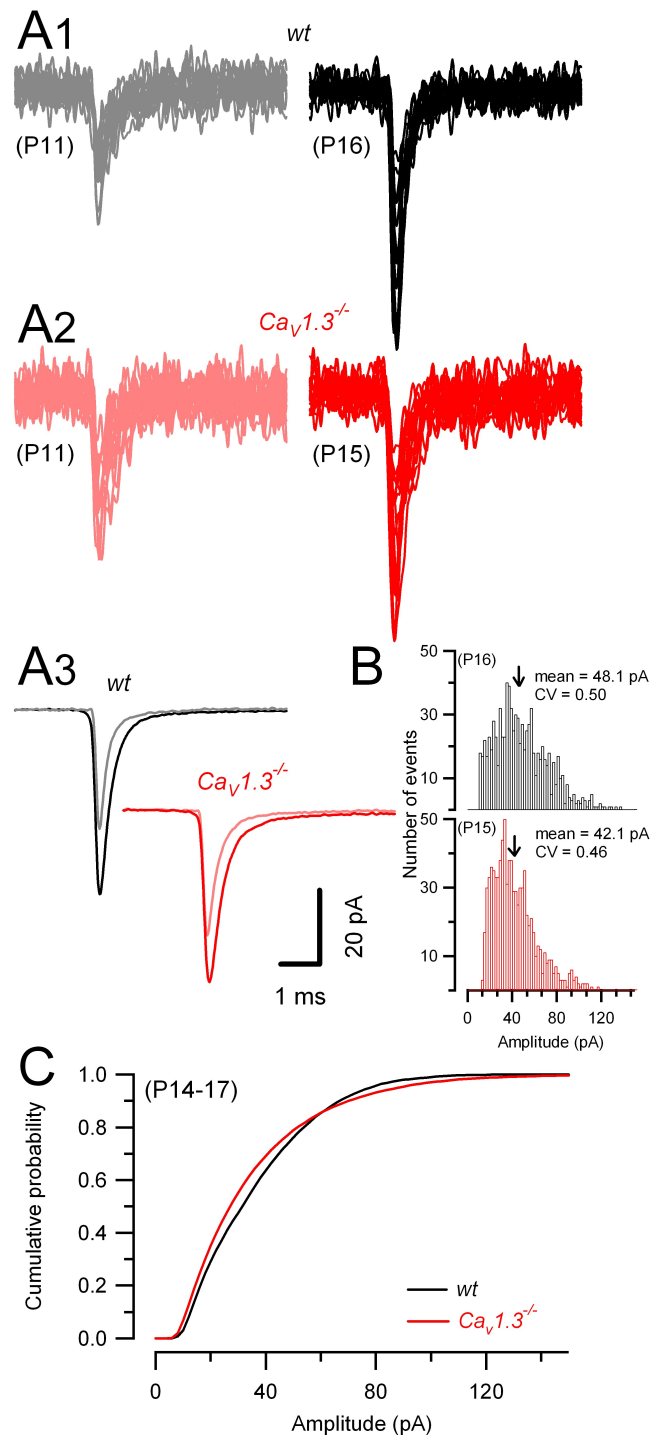
► **Figure 10. Quantal size and mEPSCs kinetics are similar in synapses of wt and $Ca_v1.3^{-/-}$ mice**

A, Representative spontaneous mEPSCs recorded at P11-16 from synapses of *wt* (grey, black, **A₁**) and $Ca_v1.3^{-/-}$ (light red, red, **A₂**) mice ($V_h = -70$ mV). **A₃**, Average mEPSC waveforms for the synapses illustrated in **A₁**, **A₂**. **B**, Representative amplitude distributions of mEPSCs in the same P15-16 cells as in **A**. Number of events are 858 and 849 for *wt* (black) and $Ca_v1.3^{-/-}$ (red) mice, respectively. Arrows indicate mean amplitudes of mEPSCs. CV, coefficient of variation (SD/mean) for the mEPSC amplitude. On average, the mEPSC peak amplitudes were similar for synapses of P14-17 $Ca_v1.3^{-/-}$ (40 ± 2.9 pA) and *wt* (43.3 ± 3.5 pA) mice. Average values of rise times and decay time constants were 88.8 μ s vs 96.8 μ s and 389 ms vs 412 ms for synapses of $Ca_v1.3^{-/-}$ vs. *wt*, respectively. **C**, Average cumulative amplitude distributions of P14-17 *wt* (black) ($n = 17$) and $Ca_v1.3^{-/-}$ (red) ($n = 29$) mice, showing comparable distributions. For each synapse, at least 500 individual mEPSCs were analyzed.

In contrast, if enhanced AMPA transmission in $Ca_v1.3^{-/-}$ mice were due purely to an increased quantal size (q), CV would remain constant (Clements, 1990; Faber and Korn, 1991). The significantly smaller ($p < 0.05$) CV in synapses of $Ca_v1.3^{-/-}$ mice (Table 1) suggests that higher quantal content contributed to the enhanced AMPA transmission.

To calculate M , we estimated q from average amplitudes of spontaneously occurring mEPSCs at the respective age (Fig. 10) (Tables 1 and 2). We observed similar developmental changes in mEPSC amplitudes in *wt* and $Ca_v1.3^{-/-}$ mice. Figure 10A shows representative traces of mEPSCs recorded from P11 and P15-16 MNTB neurons in *wt* and $Ca_v1.3^{-/-}$ cells, exhibiting a similar amplitude augmentation during development. Amplitudes of mEPSCs increased from P8 to P17 from 32 ± 1 pA ($n=8$) to 43 ± 4 pA ($n=13$) and from 36 ± 2 pA ($n=8$) to 40 ± 3 pA ($n=24$) in *wt* and $Ca_v1.3^{-/-}$ mice, respectively.

Sample amplitude histograms of mEPSCs are shown in Fig. 10B for a P16 *wt* and a P15 $Ca_v1.3^{-/-}$ synapse.



These histograms have a single peak and display a similar distribution skewed towards larger amplitudes as shown in previous studies in rat MNTB neurons (Chuhma and Ohmori, 1998; Taschenberger and von Gersdorff, 2000; Yamashita et al., 2003). They present similar mean amplitudes of mEPSCs in both *wt* and *Ca_v1.3^{-/-}* cells after the onset of hearing. Figure 10C summarizes

these results showing average cumulative amplitude distributions for P14-17 *wt* (black) and *Ca_v1.3^{-/-}* (red) cells. The two distributions were similar, although *Ca_v1.3^{-/-}* neurons seem to exhibit a slightly higher number of events with smaller amplitudes. Since the average mEPSC amplitudes were thus comparable for both groups, we estimated a 1.66 times larger average quantal content for eEPSCs in synapses of *Ca_v1.3^{-/-}* P14-17 mice.

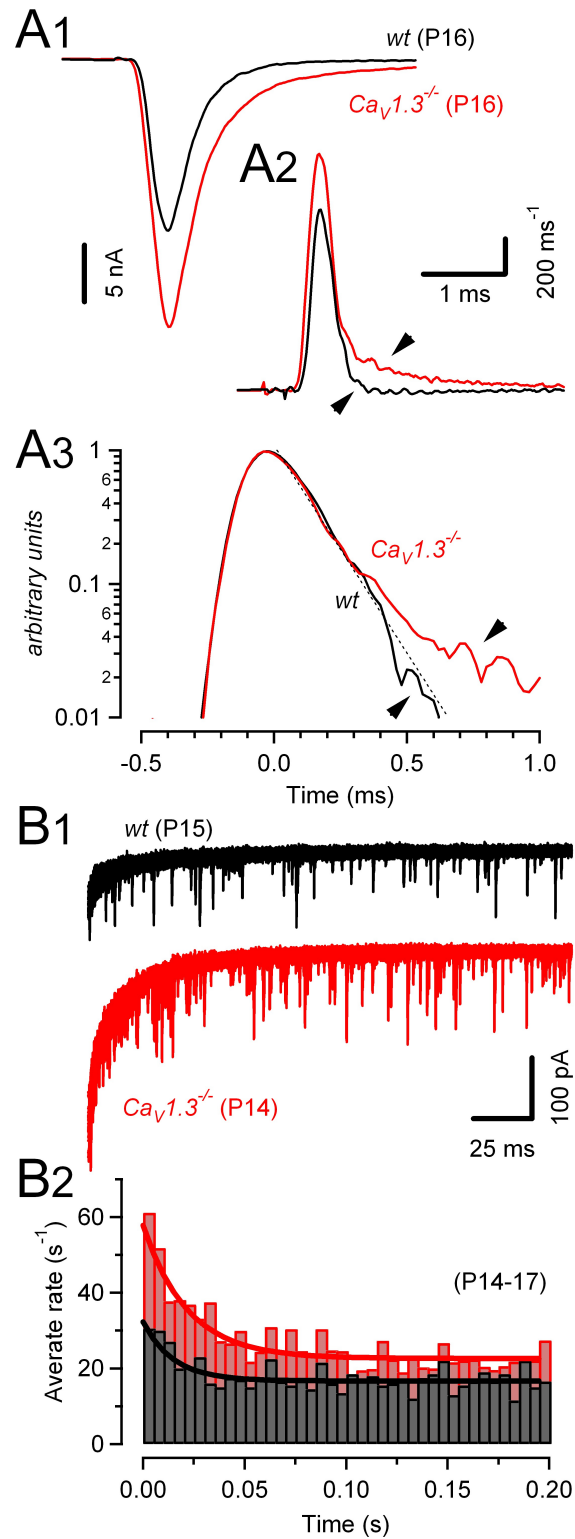
We also observed a similar development in mEPSC decay kinetics. Weighted decay time constants τ_m of mEPSCs decreased from $437 \pm 49 \mu\text{s}$ to $412 \pm 39 \mu\text{s}$ and from $497 \pm 51 \mu\text{s}$ to $389 \pm 19 \mu\text{s}$ for *wt* and *Ca_v1.3^{-/-}* mice, respectively (see also Koike-Tani et al., 2005). This result suggests that AMPA-receptor subunit composition may be unchanged in *Ca_v1.3^{-/-}* principal cells.

From P5 to P14, the time course of AP-evoked release speeds-up about 2-fold at the rat calyx of Held synapse (Taschenberger et al., 2005). For comparison, we next analyzed the time course of phasic AP-evoked release in P14-17 mouse synapses (Fig. 11A).

► **Figure 11. Time course of phasic and asynchronous release**

A, Release time course (**A2**) during EPSCs evoked by afferent-fiber stimulation was estimated by deconvolving AMPA eEPSCs (**A1**) with mEPSC waveforms obtained from the same synapse. Illustrated are two representative recordings in a *wt* (P16, *black*) and a *Ca_v1.3^{-/-}* (P16, *red*) mouse. **A3**, Average release functions obtained from 10 *wt* (*black*) and 9 *Ca_v1.3^{-/-}* (*red*) mice plotted on a semi-log scale. Peak amplitudes of the release function were normalized and aligned at $t = 0$ ms before averaging. Only synapses with peak amplitudes ≤ 15 nA were included in this dataset to avoid complications due to non-linear summation of quantal currents because of receptor saturation. Except for a small deviation during the late phase (indicated by the arrow heads in **A2** and **A3**), the kinetics of AP-evoked release in *Ca_v1.3^{-/-}* mice were similar to that in P14-17 *wt* mice. Dotted line was fitted by eye and represents a single exponential decay with $\tau = 140 \mu\text{s}$. **B1**, Asynchronous release after conditioning trains of 10 EPSCs (100 Hz) in a P15 *wt* (*black*) and a P14 *Ca_v1.3^{-/-}* (*red*) mouse. **B2**, Pooled data from 4 *wt* (*black*) and 5 *Ca_v1.3^{-/-}* (*red*) mice. Immediately after the conditioning trains, asynchronous release was transiently elevated. Peak release rates were on average nearly two times higher in *Ca_v1.3^{-/-}* mice ($61.1 \pm 4.6 \text{ s}^{-1}$ vs $32.7 \pm 4.8 \text{ s}^{-1}$) ($p < 0.05$).

Deconvolution of AMPA eEPSCs with average single vesicle responses (mEPSCs) obtained from the same synapses was carried out in the frequency domain using FFT routines (Diamond and Jahr, 1995; Hefft and Jonas, 2005).



Such analysis implies that for single eEPSCs any current component activated by glutamate spillover is negligible at this age (but see Neher and Sakaba, 2001a).

With an average half-width of $263 \pm 18 \mu\text{s}$ ($n=10$) and $253 \pm 21 \mu\text{s}$ ($n=9$) for *wt* and *Ca_v1.3^{-/-}* synapses, respectively, the kinetics of the release transient was considerably faster for P14-17 mouse calyx of Held synapses compared to values reported before for rat calyces at different developmental stages (Fig. 11A3) (Bollmann et al., 2000; Schneggenburger and Neher, 2000; Taschenberger et al., 2005).

Whereas rise and initial decay of the release transient were virtually indistinguishable between *wt* and *Ca_v1.3^{-/-}* mice, we notice the presence of a late and more slowly decaying component in the latter. This additional slow release component is consistent with the slightly slower decay of EPSC_{AMPA} in *Ca_v1.3^{-/-}* mice (Table 1) and may reflect late release due to the broader calyceal APs (Fig. 8A). Alternatively, it may represent glutamate spillover caused by the higher average quantal content of eEPSCs in synapses of *Ca_v1.3^{-/-}* mice (see below).

As described above, we estimated the Ca^{2+} influx during single calyceal APs of *Ca_v1.3^{-/-}* mice to be slightly larger compared with *wt* mice. During AP trains such elevated Q_{Ca} may accumulate and, assuming similar Ca^{2+} buffering and extrusion kinetics in *wt* and *Ca_v1.3^{-/-}* mice, result in higher residual Ca^{2+} levels in the latter. Asynchronous release driven by such temporarily elevated Ca^{2+} after high frequency stimulation may therefore differ between *wt* and *Ca_v1.3^{-/-}* synapses. To evaluate this possibility we quantified the rates of asynchronously released quanta after 100 Hz trains consisting of 10 EPSCs (Fig. 11B).

Asynchronous release events following such stimulus trains were superimposed on a slowly decaying postsynaptic current component (Fig. 11B1). The latter could be fitted by a double-exponential function having a fast time constant of a few ms (*wt*: 5 ± 0.8 ms, $Ca_v1.3^{-/-}$: 4 ± 0.4 ms) probably reflecting the slow component of AMPA EPSC decay and a slow time constant of several tens of ms (*wt*: 46 ± 5 ms, $Ca_v1.3^{-/-}$: 30 ± 3 ms) presumably reflecting the clearance of residual glutamate (Taschenberger et al., 2005) and/or deactivation of a small NMDA EPSC component.

The frequencies of spontaneously occurring mEPSCs were comparable between synapses of *wt* and those of $Ca_v1.3^{-/-}$ mice (Table 1), but slightly higher than previously reported for P12-14 rats (Taschenberger et al., 2005). Consistent with the latter study, we found that asynchronous release after trains increased only little over the rate of spontaneous release in *wt* mice. In contrast, in synapses of $Ca_v1.3^{-/-}$ mice, asynchronous release increase transiently to a two fold higher average rate (Fig. 11B2) before quickly decaying back to the resting rate (decay time constant $\tau_{\text{decay}} = 15 \pm 3$ ms and 22 ± 4 ms for *wt* [$n = 4$] and $Ca_v1.3^{-/-}$ [$n = 5$], respectively). This behavior is reminiscent of increased asynchronous release reported for endbulb synapses in the anteroventral cochlear nucleus of congenitally deaf mice (Oleskevich and Walmsley, 2002).

3.6 Elevated release probability in calyx of Held synapses of $Ca_v1.3^{-/-}$ mice

Higher quantal content observed for AP-evoked EPSCs in $Ca_v1.3^{-/-}$ synapses may be caused by an increased fraction (F) of readily releasable quanta consumed by a single AP and/or a larger total number of vesicles available for release (RRP). Presynaptic capacitance recordings yielded no evidence in favor

of the latter whereas the slightly broader AP waveform in $Ca_v1.3^{-/-}$ mice is consistent with an increased F (Fig. 8). We therefore sought to compare F between P14-17 synapses of *wt* and $Ca_v1.3^{-/-}$ mice.

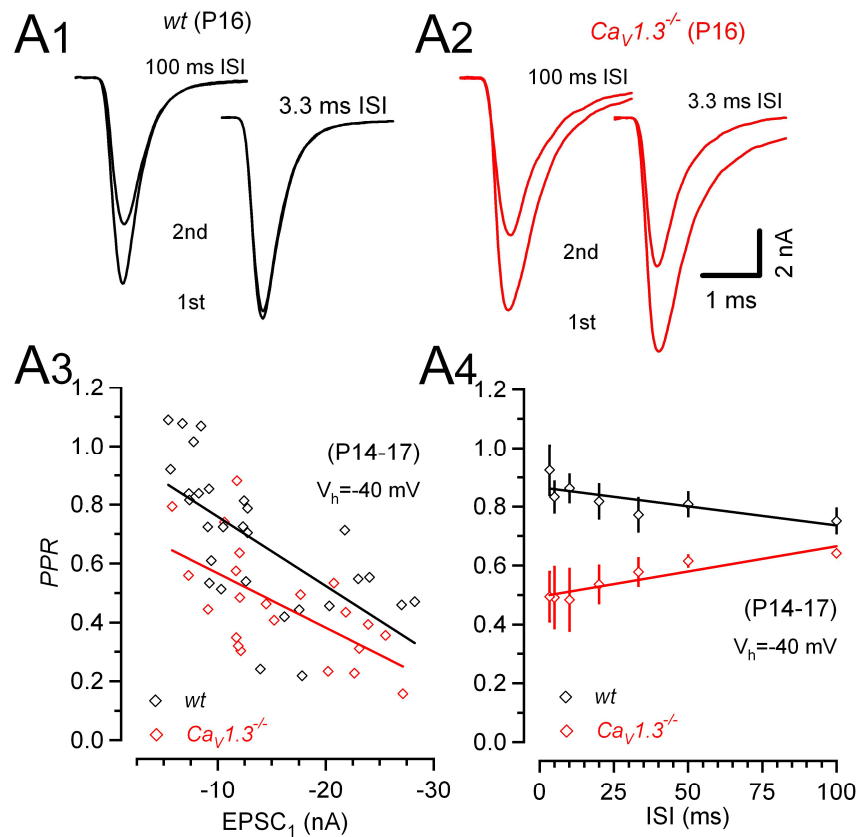


Figure 12. PPR estimates higher probability of release in $Ca_v1.3^{-/-}$ mice

A, Paired pulse ratios for various inter-stimulus intervals (ISIs) of P14-17 synapses of *wt* (*black*) and $Ca_v1.3^{-/-}$ (*red*) mice. Representative recordings from a P16 *wt* (**A1**) and P16 $Ca_v1.3^{-/-}$ (**A2**) mouse are shown. **B1**, Scatter plot of *PPRs* vs. $EPSC_1$ amplitude (ISI = 10 ms) for *wt* (*red*) and $Ca_v1.3^{-/-}$ mice, illustrating strong correlation between initial EPSC size and measured paired-pulse depression (*wt*: $n = 29$, $r = 0.649$, $p < 0.001$, $Ca_v1.3^{-/-}$: $n = 22$, $r = 0.624$, $p = 0.002$). **B2**, *PPRs* were generally smaller in $Ca_v1.3^{-/-}$ mice indicative of a higher release probability. With increasing ISIs, *PPRs* decreased in *wt* ($n = 8$, $r = -0.771$, $p = 0.05$) but increased in $Ca_v1.3^{-/-}$ ($n=8$, $r = 0.924$, $p = 0.002$) mice. Linear regressions in (**B1**) and (**B2**) are represented by the solid lines.

Changes in F often correlate with changes in paired pulse ratio ($PPR = EPSC_2/EPSC_1$) (Debanne et al., 1996; Dobrunz and Stevens, 1997; Oleskevich

et al., 2000). For inter-stimulus intervals (ISIs) of 10 ms, we found a strong correlation between the size of EPSC₁ and *PPR* among synapses from *wt* and *Ca_v1.3^{-/-}* mice (Fig. 12B1). When measured for various ISIs (100 ms - 3.3 ms), *PPRs* were consistently lower in *Ca_v1.3^{-/-}* synapses, indicative of higher *F*. In *wt* synapses, *PPRs* increased slightly from 0.75 to 0.92 with decreasing ISI presumably due to a facilitation of EPSC₂. In contrast, *PPRs* declined with decreasing ISI in *Ca_v1.3^{-/-}* synapses (from 0.64 to 0.49) perhaps because of AMPAR desensitization starting to contribute to the reduction of EPSC₂ (Fig. 12B2).

Assuming that the measured paired-pulse depression resulted purely from vesicle depletion and neglecting other contributions that may affect *PPR* such as presynaptic facilitation and postsynaptic receptor desensitization, we can approximate *F* according to

$$F = (1 - PPR)e^{\frac{\Delta t}{\tau}}$$

where Δt represents the inter-stimulus interval and τ the time constant of recovery from vesicle depletion. Analyzing the *PPRs* obtained using ISIs of 100 to 50 ms for which the contribution of postsynaptic receptor desensitization is expected to be small at this age (Taschenberger et al., 2005) and synaptic facilitation has decayed to a minimum, we obtained $F = 0.24-0.19$ and $F = 0.33-0.39$ for *wt* ($n = 9$) and *Ca_v1.3^{-/-}* ($n = 9$) synapses, respectively. A similar analysis carried out in P8-11 synapses yielded larger *F* estimates (0.44-0.46 and 0.47-0.55 for *wt* [$n = 12$] and *Ca_v1.3^{-/-}* [$n = 7$] synapses, respectively) consistent with a developmental decrease in release probability as reported for the rat (Iwasaki and Takahashi, 2001; Taschenberger et al., 2002).

We emphasize that these F values may represent upper limits if AMPAR desensitization contributed to the relative reduction of EPSC₂ especially in $Ca_v1.3^{-/-}$ mice where M was high. Vesicle recruitment during the 33 - 50 ms ISI is negligible because after synaptic depression induced by conditioning 100 Hz trains we measured slow recovery time constants of 3-6 s (P8-11: 3.9 ± 0.3 s and 3.5 ± 0.4 s, P14-17: 5.9 ± 0.8 s and 3.4 ± 0.5 s for wt and $Ca_v1.3^{-/-}$ mice, respectively) throughout development (but see Joshi and Wang, 2002).

Figure 13 show recovery from synaptic depression in P14-17 synapses of wt and $Ca_v1.3^{-/-}$ mice. A conditioning train of 15 stimuli at 100 Hz was followed by a single test pulse given at a variable time interval after the end of the stimulus train (Fig. 13A). A waiting period of 20 s plus the time interval was used between the single test pulse and a subsequent conditioning train. Notice the higher extent of synaptic depression (Fig. 13A), but faster vesicle replenishment (Fig. 13B) in $Ca_v1.3^{-/-}$ MNTB neurons.

Vesicle release probability can also be calculated as the fraction of released vesicles by a single action potential from a total pool of available vesicles. In P14-17 synapses, where desensitization and AMPA-receptor saturation are negligible (Taschenberger et al., 2002; Yamashita et al., 2003; Taschenberger et al., 2005), the number of readily releasable vesicles, N , may be estimated by summing up peak EPSC amplitudes during trains at high stimulation frequencies (Schneppenburger et al., 1999; Bollmann et al., 2000; Taschenberger and von Gersdorff, 2000; Iwasaki and Takahashi, 2001; Taschenberger et al., 2002).

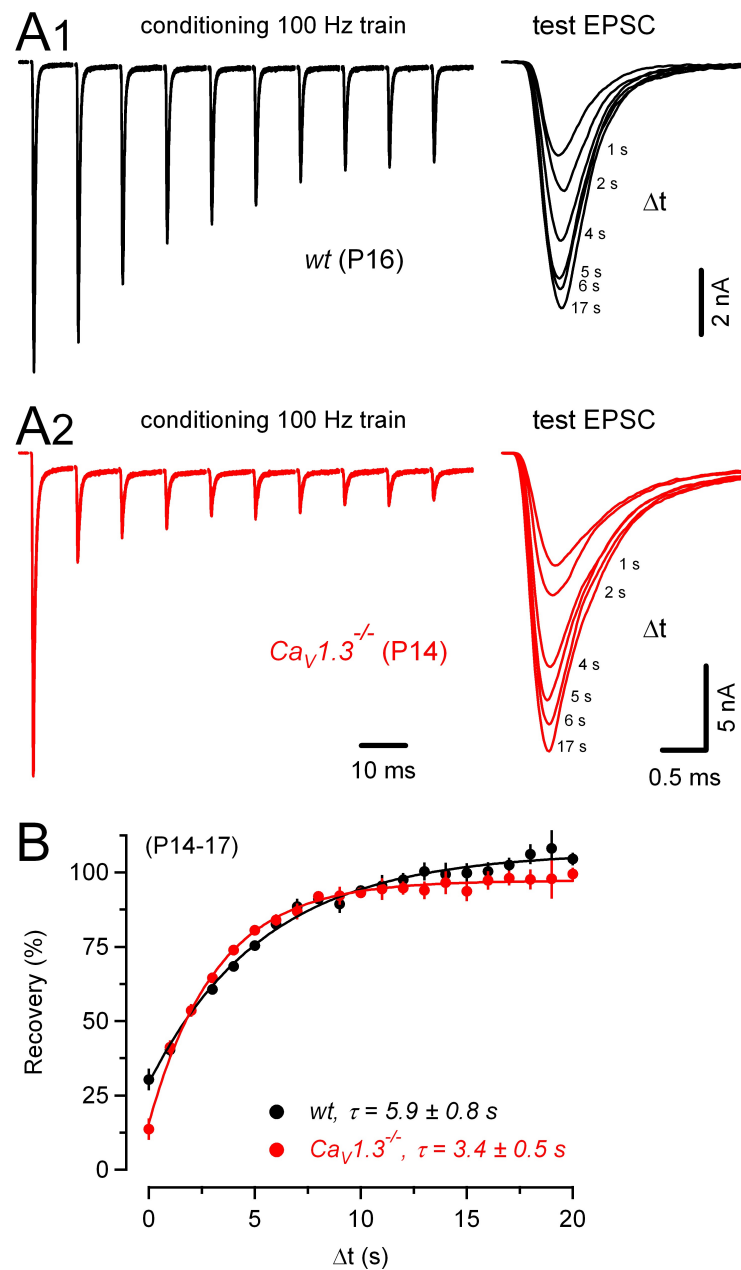


Figure 13. Recovery from synaptic depression after 100 Hz trains is slightly faster in $Ca_v1.3^{-/-}$ mice

A, *Left*, superimposed representative trains consisting of 10 EPSCs evoked by afferent fiber stimulation (100 Hz) in a P16 *wt* (*black*, **A₁**) and a P14 $Ca_v1.3^{-/-}$ (*red*, **A₂**) postsynaptic cells. *Right*, test EPSCs were evoked at different intervals (ranging from 1 s to 20 s) following a conditioning train (*left*). Representative traces of test EPSCs are shown in intervals of 1, 2, 4, 5, 6 and 17 s for the same cells as in *left panel*. An inter-sweep interval of 20 s plus the test interval was sufficient to allow full recovery from synaptic depression. **B**, Recovery is expressed as $(I_{test}) / (I_{1st}) * 100$, where I_{test} is the peak amplitude of the test EPSCs and I_{1st} is the peak amplitude of the first EPSC of the conditioning train. Recovery time course was fitted by single exponentials. Time constant of the fitted exponentials were faster in $Ca_v1.3^{-/-}$ than in *wt* synapses (see graph legend). $V_h = -40$ mV.

Figure 14A shows average cumulative plots of peak EPSC amplitudes for P8-11 and P14-17 *wt* and *Ca_v1.3^{-/-}* neurons, after afferent fiber stimulation at 100 Hz (15 stimuli). Cumulative plots were fitted with a line for the last three points (dotted lines) and back-extrapolated to 0 to estimate pool sizes. We obtained values of vesicle pool sizes proportional to -25.4 nA (1026 vesicles) and -30.2 nA (1321 vesicles) for P14-17 *wt* and *Ca_v1.3^{-/-}* mice, respectively. First EPSC amplitudes from the same trains used to build cumulative plots averaged -10.4 nA and -15.8 nA for P14-17 *wt* and *Ca_v1.3^{-/-}* cells. Therefore vesicle release probabilities resulted in values of 0.41 and 0.52 in P14-17 *wt* and *Ca_v1.3^{-/-}* synapses, respectively.

This analysis is similar to the one first applied in the neuromuscular junction by (Elmqvist and Quastel, 1965) (Fig. 14B). When EPSCs are plotted vs. cumulative release, an extrapolation of a line fitted to the first EPSC amplitudes in a train provides an estimate for the total amount of releasable quanta. For P14-17 *wt* and *Ca_v1.3^{-/-}* cells, the estimates of N using the latter method were proportional to -32.6 nA (1317 vesicles) and -30.6 nA (1338 vesicles), respectively. This yielded values of P_{ves} of 0.32 and 0.52 for *wt* and *Ca_v1.3^{-/-}* neurons, respectively. Altogether, these results suggest an elevated vesicle release probability in calyces of *Ca_v1.3^{-/-}* compared to *wt* mice.

Increased release probability may also be associated with a faster progressive block of EPSC_{NMDA} by the use-dependent NMDAR antagonist MK-801 (Hessler et al., 1993; Rosenmund et al., 1993; Iwasaki and Takahashi, 2001; de Lange et al., 2003).

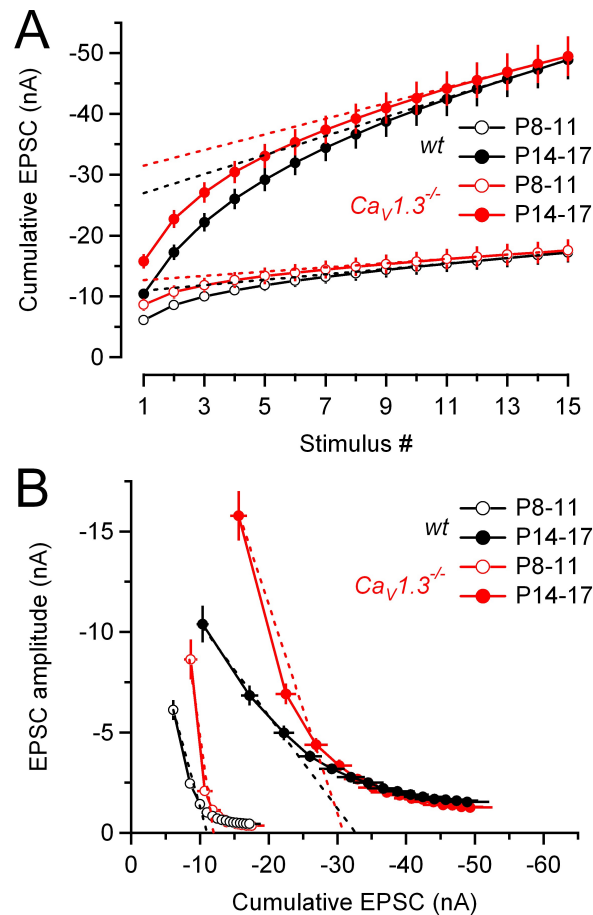
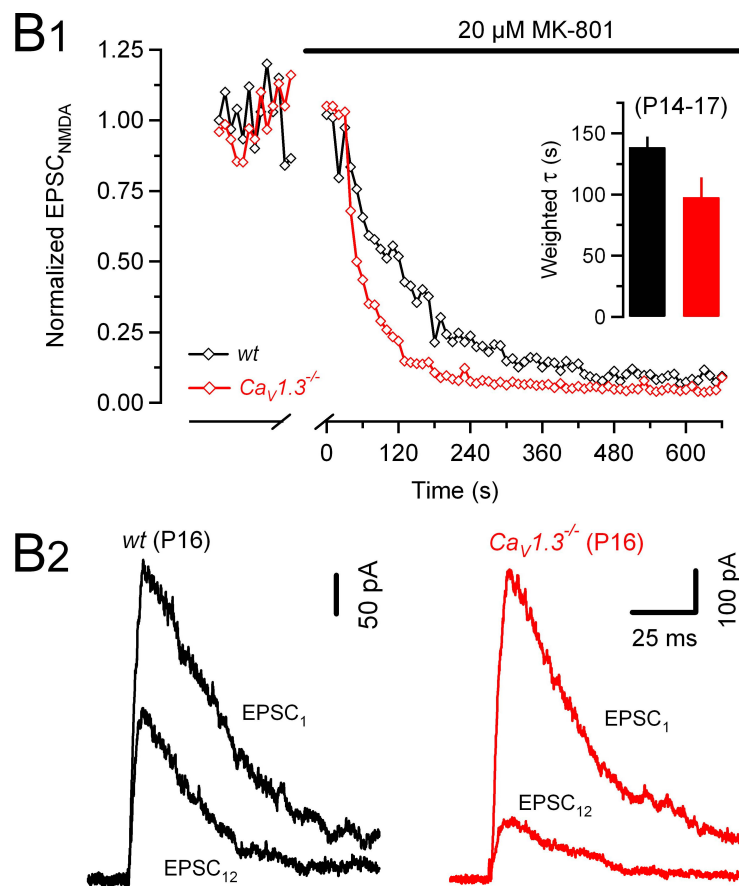


Figure 14. Estimates for pool size show comparable number of available vesicles

A, Cumulative EPSC amplitudes of 100 Hz trains in P8-11 (*open circles*) and P14-17 (*filled circles*) *wt* (*black*) and $Ca_v1.3^{-/-}$ (*red*) mice were obtained by adding EPSC amplitudes to estimate change in vesicle pool sizes. Dotted lines represent linear fits to the last three EPSC amplitudes during the train, back-extrapolated to 0 to estimate the cumulative EPSC amplitudes before steady-state depression. **B**, Elmqvist-Quastel plot for the same data as in **A** to estimate probability of release of a single quantum (P_{ves} , see text). Line fit to the first three points; extrapolation to 0 nA of EPSC amplitude shows the initial vesicle pool size. Recordings were made at $V_h = -40$ mV.

To corroborate a hypothesized higher release probability in $Ca_v1.3^{-/-}$ mice, we measured the blocking rate of NMDA EPSCs at $V_h = 40$ mV and in the presence of 2 μ M NBQX to completely abolish AMPA currents (Fig. 15). After acquiring control NMDA EPSCs, stimulation was stopped and 20 μ M MK-801 were added to the bath. Stimulation was resumed about 2 min later.

During 0.1 Hz stimulation, EPSC_{NMDA} declined exponentially in the presence of MK-801 with an average time constant of 139 ± 8 s in *wt* synapses and 98 ± 15 s in *Ca_v1.3^{-/-}* synapses ($p < 0.05$, Fig. 15A). Representative examples of NMDA EPSCs recorded in control ringers and after eliciting 12 presynaptic APs in MK-801 containing bath solution are shown in Fig. 15B. Together with the decreased *PPRs* and estimates of pool size, these results support an elevated release probability in *Ca_v1.3^{-/-}* synapses.

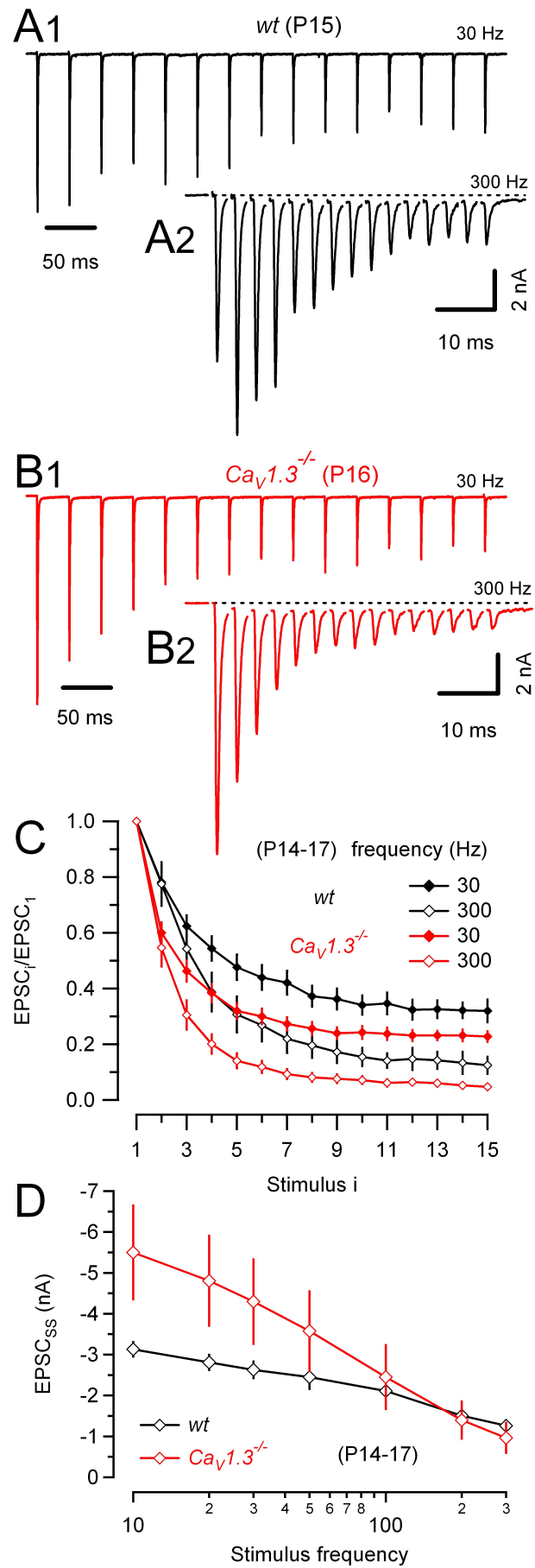


Mature calyx of Held synapses can reliably operate at frequencies of several hundreds of Hz (Wu and Kelly, 1993). A developmental reduction of F (Iwasaki and Takahashi, 2001; Taschenberger et al., 2002) seems to be beneficial in order to achieve such high transmission rates.

When measuring eEPSC trains elicited by high-frequency stimulation (Fig. 16) we notice significantly stronger synaptic depression in $Ca_v1.3^{-/-}$ synapses. In contrast, synaptic depression was frequently converted to facilitation of the initial eEPSCs when stimulating *wt* synapses with frequencies of 100 Hz and above (compare Figs. 16A2 and B2). Average results for 7-10 *wt* and 8-12 $Ca_v1.3^{-/-}$ synapses are illustrated in Fig. 16C. Both stimulation frequencies (30 and 300 Hz) resulted in significantly stronger synaptic depression in synapses which developed in the absence of cochlea-driven afferent nerve activity. Steady state amplitudes (EPSC_{SS}) obtained from the average of the last three EPSCs during the trains are plotted vs. stimulation frequency in Fig. 16D. EPSC_{SS} declined much steeper with increasing stimulation frequency in $Ca_v1.3^{-/-}$ compared with *wt* synapses.

◀ **Figure 15. Faster blocking time course of NMDA EPSCs by MK-801 suggests a higher probability of release in $Ca_v1.3^{-/-}$ mice**

A, NMDA EPSCs recorded at $V_h = +40$ mV (stimulation frequency 0.1 s^{-1}) in the presence of $2\text{ }\mu\text{M}$ NBQX to completely block AMPA currents. After a period of recording control EPSCs for 3 min, stimulation was stopped and perfusion was switched to MK-801 ($20\text{ }\mu\text{M}$) containing bath solution. MK-801 was allowed to equilibrate in the recording chamber for 2 minutes before resuming fiber stimulation. The blocking time course was then recorded for another 15 min. Blocking was faster in the P16 $Ca_v1.3^{-/-}$ (*red*) compared with the P16 *wt* (*black*) mouse. Average values of the weighted time constants are compared in the inset bar graph. **B**, First and 12th NMDA EPSCs recorded during MK-801 application superimposed for comparison. Note the more complete block in the synapse from a $Ca_v1.3^{-/-}$ (*red*) compared with the *wt* (*red*) mouse.



◀ Figure 16. Stronger synaptic depression in $Ca_v1.3^{-/-}$ mice

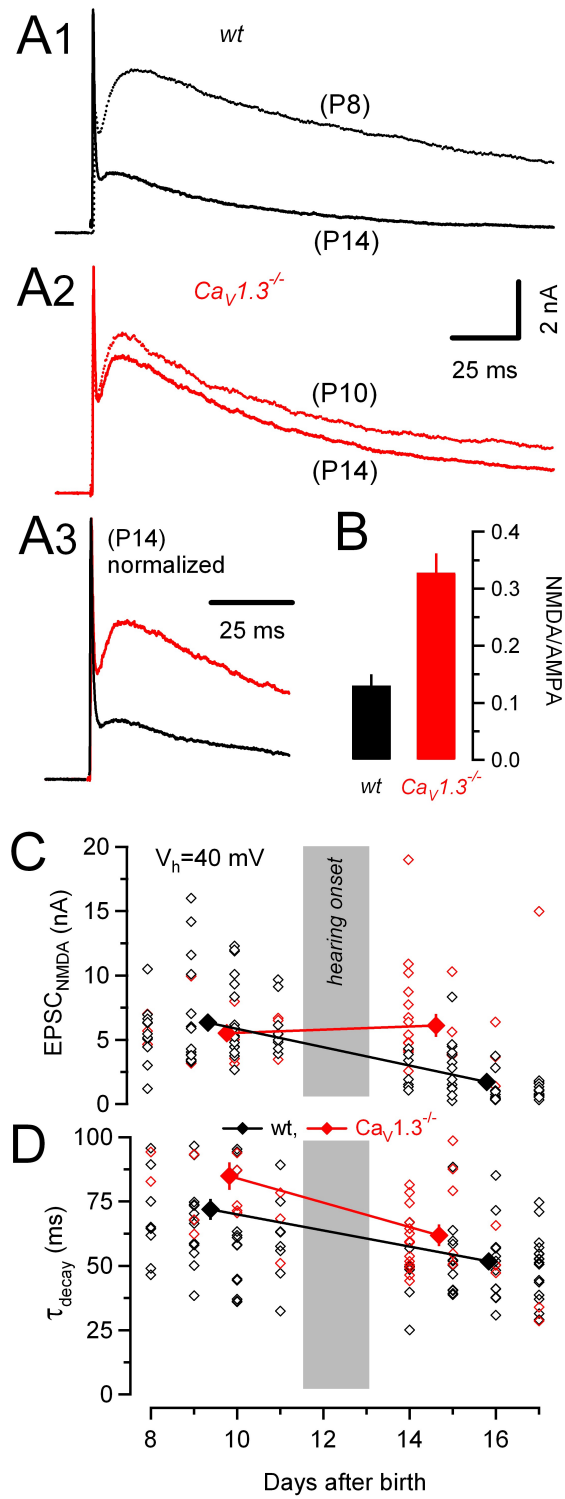
A,B, Trains of 15 EPSCs evoked by afferent-fiber stimulation in a *wt* (**A**) and a $Ca_v1.3^{-/-}$ (**B**) mouse using stimulus frequencies of 30 Hz (**A1,B1**) and 300 Hz (**A2,B2**). Dotted lines in (**A2**) and (**B2**) represent baseline current (0 pA) and are shown to indicate a sustained eEPSC component which slowly developed during high-frequency trains and presumably reflects AMPAR and/or NMDAR activation by residual glutamate. **C**, Pooled data for *wt* (*black*, n= 7-10) and $Ca_v1.3^{-/-}$ (*red*, n= 8-12) mice. EPSC amplitudes were normalized to the peak amplitude of the initial eEPSCs. Note the stronger depression in $Ca_v1.3^{-/-}$ mice for both stimulus frequencies. **D**, Steady state EPSC amplitudes vs. stimulus frequency. In $Ca_v1.3^{-/-}$ mice, EPSC_{ss} was almost two-fold larger for low-frequency stimulation but declined more steeply with increasing frequency. EPSC_{ss} was estimated from the average amplitude of the last three EPSCs during the trains.

3.7 Delayed down-regulation of synaptic NMDA receptors in

$Ca_v1.3^{-/-}$ mice

During early postnatal development of the rat and mouse calyx of Held synapse, NMDA EPSC (EPSC_{NMDA}) amplitudes decrease steeply (Taschenberger and von Gersdorff, 2000; Futai et al., 2001; Joshi and Wang, 2002). Since cochlear ablation retards this down-regulation (Futai et al., 2001), the latter process is likely to be, at least in part, controlled by cochlea-driven nerve activity. We therefore compared the properties of EPSC_{NMDA} recorded before and after the onset of hearing in synapses of *wt* mice with those recorded in $Ca_v1.3^{-/-}$ mice (Fig. 17,18).

Amplitudes of *wt* NMDA EPSCs decreased during development similarly as described before (from 6.34 ± 0.44 nA [n = 52] to 1.72 ± 0.23 nA [n = 50], Fig. 17A,C) (Futai et al., 2001; Joshi and Wang, 2002) whereas in $Ca_v1.3^{-/-}$ mice their average amplitudes slightly increased (from 5.52 ± 0.46 nA [n = 17] to 6.10 ± 0.79 nA [n = 27]).



To test whether enhanced release can fully account for the larger EPSC_{NMDA} size in *Ca_v1.3^{-/-}* mice we measured EPSC_{NMDA}/EPSC_{AMPA} ratios in a subset of P14-17 synapses. This ratio was significantly higher ($p < 0.001$) in *Ca_v1.3^{-/-}* mice suggesting differences in postsynaptic receptor expression (Fig. 17B).

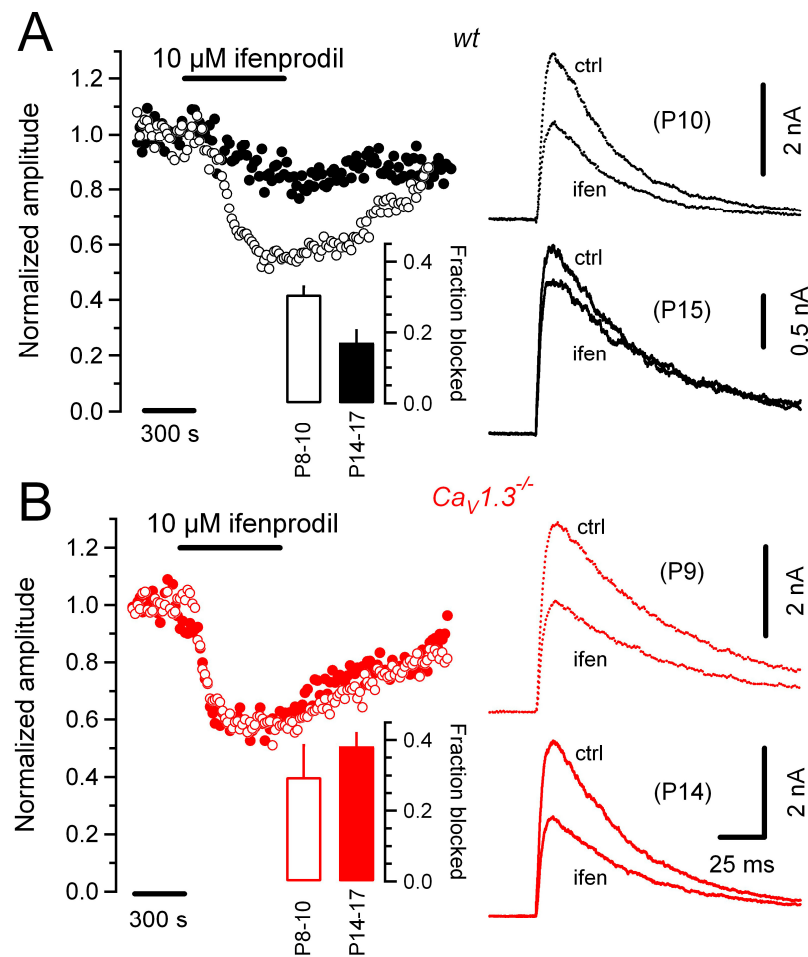
A small acceleration of the decay kinetics of NMDA EPSCs was seen in both groups during postnatal development from P8 to P17 (Fig. 17D). The decay of EPSC_{NMDA} was ~25% faster at P14-17 (Table 1) compared with P8-11 (Table 2) (*wt*: 72 ± 4 ms, $n = 52$, *Ca_v1.3^{-/-}*: 85 ± 5 ms, $n = 17$).

In many central glutamatergic synapses, the relative loss of synaptic NMDARs correlates with changes in subunit expression (Williams et al., 1993; Monyer et al., 1994; Sheng et al., 1994; Shi et al., 1997; Liu et al., 2004). To test for such developmental regulation we made use of the NR2B subtype-specific NMDA antagonist ifenprodil (Williams, 1993; Tovar and Westbrook, 1999).

◀ **Figure 17. Delayed developmental decrease of NMDA EPSCs in *Ca_v1.3^{-/-}* mice**

A, EPSCs recorded at $V_h = +40$ mV in MNTB synapses of *wt* (**A1**, black) and *Ca_v1.3^{-/-}* (**A2**, red) mice before (*broken lines*) and after (*solid lines*) hearing onset. At P14, NMDA EPSCs were strongly reduced in synapses of *wt* but not in those of *Ca_v1.3^{-/-}* mice. Pipettes were filled with CsCl-based solution containing 5 mM EGTA. **A3**, same traces after normalizing their AMPA EPSC peak amplitudes to compare NMDA/AMPA EPSC ratios. **B**, Average values of NMDA/AMPA EPSC ratios for P14-17 synapses were significantly larger in *Ca_v1.3^{-/-}* mice (*red*). EPSC amplitudes were measured at $V_h = -40$ mV (EPSC_{AMPA}) and $V_h = +40$ mV (EPSC_{NMDA}). **C**, Scatter plot of EPSC_{NMDA} vs. age. During development, NMDA EPSC peak amplitudes decreased strongly in synapses of *wt* (*black*) but not in those of *Ca_v1.3^{-/-}* mice (*red*). EPSC_{NMDA} was measured >10 ms after the AMPA EPSC peak when the fast EPSC component had decayed to <1% of its peak. At P14-17, average peak amplitudes of EPSC_{NMDA} were more than three times larger in *Ca_v1.3^{-/-}* (6.1 ± 0.79 nA, $n = 27$) compared with *wt* synapses (1.7 ± 0.23 nA, $n = 50$). **D**, Decay time constants of EPSC_{NMDA} decreased slightly less in *Ca_v1.3^{-/-}* than in *wt* mice during development.

As shown in Fig. 18A, the sensitivity of EPSC_{NMDA} to ifenprodil (10 μ M) decreased during development in *wt* synapses (from $30.6 \pm 2.2\%$ [$n = 18$] to $17.2 \pm 3.5\%$ [$n = 14$] block, $p < 0.01$). In *Ca_v1.3^{-/-}* mice, the average block by ifenprodil was slightly larger at P14-17 ($38.2 \pm 3.7\%$, $n=7$) compared with P8-11 ($29.5 \pm 9.0\%$, $n=4$), although this increase was statistically not significant ($p=0.32$) (Fig. 18B).



Taken together these data suggest that afferent nerve activity promotes a preferential pruning of NR2B subunit-containing NMDARs from subsynaptic sites (Lindlbauer et al., 1998). This pruning process seems delayed in the absence of cochlea-driven afferent nerve activity. NR2A and NR2B subunits confer different kinetic properties to the NMDAR channel (Monyer et al., 1994; Takahashi et al., 1996). However, because of the almost similar developmental acceleration of the NMDA EPSC decay kinetics seen in both *wt* as well as *Ca_v1.3^{-/-}* mice (Fig. 17D), it is more likely that the faster decay time constants measured in P14-17 synapses relate to the speed-up of transmitter clearances at the calyx of Held synapse (Taschenberger et al., 2005) rather than to changes in NMDAR subunit composition.

◀ **Figure 18. Persistent sensitivity of EPSC_{NMDA} to the NR2B specific antagonist ifenprodil in synapses of *Ca_v1.3^{-/-}* mice**

A, Inhibition by ifenprodil (10 μ M) of NMDA EPSCs in *wt* synapses before (P8, open circles) and after (P15, filled circles) hearing onset. Individual traces recorded before and after drug application are shown superimposed in the right panel. Bath application of ifenprodil resulted in a robust decrease of NMDA EPSCs in P8-11 synapses of *wt* mice (inset, open bar, $n = 18$). The fractional block was largely reduced at P14-17 (inset, filled bar, $n = 14$). B, Similar experiments as illustrated in (A) in *Ca_v1.3^{-/-}* mice (P9, open circles, P14, filled circles). In synapses from *Ca_v1.3^{-/-}* mice, the sensitivity to ifenprodil persisted throughout development, suggesting expression of a larger fraction of NR2B subunit-containing NMDARs even at P14-17. Average block was 30% (inset, open bar, $n = 4$) and 38% (inset, filled bar, $n = 7$) for P8-11 and P14-17 *Ca_v1.3^{-/-}* mice, respectively. In all experiments illustrated in (A,B), the bath solution contained 2 μ M NBQX to completely block EPSC_{AMPA} and V_h was +40 mV.

Table 1. Functional properties of synaptic transmission in **P14-17** calyx of Held synapses of $Ca_v1.3^{-/-}$ compared to those of *wt* mice. Number of synapses tested is given in parenthesis. (n.s. = not significant; values are given as mean \pm SEM)

Parameter	<i>wt</i>	$Ca_v1.3^{-/-}$	
calyceal $I_{Ca(V)}$			
amplitude (@ 0 mV) (nA)	1.20 \pm 0.14 (9)	1.23 \pm 0.08 (11)	n.s.
facilitation (@ 200Hz)			
amplitude (%)	42.0 \pm 6.2 (8)	33.0 \pm 5.7 (9)	n.s.
$\tau_{facilitation}$ (ms)	9.7 \pm 1.1 (8)	9.8 \pm 2.0 (9)	n.s.
calyceal AP			
half-width (μ s)	193.4 \pm 8.9 (14)	222.1 \pm 8.4 (16)	p<0.05
amplitude (mV)	139.4 \pm 1.9 (14)	139.3 \pm 3.0 (16)	n.s.
EPSC_{AMPA}			
amplitude (nA) ^a	11.20 \pm 0.79 (55)	17.20 \pm 1.02 (50)	p<0.001
CV	0.080 \pm 0.007	0.052 \pm 0.006	p<0.05
rise time (20-80%) (ms) ^b	0.14 \pm 0.01 (17)	0.15 \pm 0.01 (14)	n.s.
decay ^b			
τ_{fast} (ms)	0.34 \pm 0.02 (16)	0.37 \pm 0.02 (14)	n.s.
τ_{slow} (ms)	2.93 \pm 0.27 (16)	2.63 \pm 0.27 (14)	n.s.
a_{fast} (%) ^c	95.8 \pm 0.5 (16)	89.9 \pm 1.4 (14)	p<0.01
weighted τ_m (ms) ^d	0.46 \pm 0.03 (16)	0.57 \pm 0.06 (14)	p<0.05
recovery time constant (s) ^e	5.9 \pm 0.8 (8)	3.4 \pm 0.5 (10)	p<0.05
mEPSC			
frequency (s ⁻¹)	11 \pm 2 (17)	14 \pm 1 (29)	n.s.
amplitude (pA)	43.3 \pm 0.4 (13)	40.1 \pm 0.3 (24)	n.s.
rise time (20-80%) (μ s)	96.8 \pm 4.9 (13)	88.8 \pm 2.3 (24)	n.s.
decay time constant (ms)			
τ_{fast}	0.29 \pm 0.02 (13)	0.25 \pm 0.01 (24)	n.s.
τ_{slow}	1.53 \pm 0.19 (13)	1.21 \pm 0.09 (24)	n.s.
a_{fast} (%) ^c	88.1 \pm 2.1 (13)	84.7 \pm 0.9 (24)	n.s.
weighted τ_m (ms) ^d	0.41 \pm 0.04 (13)	0.39 \pm 0.02 (24)	n.s.
Quantal parameters			
F^f	0.31 \pm 0.04 (28)	0.50 \pm 0.04 (24)	p<0.01
RRP^f	1623 \pm 147 (28)	1829 \pm 423 (24)	n.s.
EPSC_{NMDA}			
amplitude (nA) ^g	1.72 \pm 0.23 (50)	6.10 \pm 0.79 (27)	p<0.001
decay time constant (ms) ^g	51.8 \pm 2.2 (49)	61.8 \pm 3.8 (25)	p<0.05
EPSC _{NMDA} /EPSC _{AMPA} ^h	0.13 \pm 0.02 (35)	0.33 \pm 0.03 (24)	p<0.001
ifenprodil block (%)	17.2 \pm 3.5 (14)	38.2 \pm 3.7 (7)	p<0.01

^a Measured at $V_h = -40$ mV; ^b measured at $V_h = -70$ mV; ^c Relative amplitude of the fast decay component; ^d weighted mean decay time constant $\tau_m = a_{fast} * \tau_{fast} + a_{slow} * \tau_{slow}$, where a_{fast} and a_{slow} are the relative amplitudes of the fast and slow decay components, respectively; ^e time course of recovery from depression was estimated using conditioning 100 Hz trains; ^f estimated from synaptic depression during 100 Hz trains (Taschenberger et al., 2002); ^g measured at $V_h = +40$ mV; ^h EPSC_{NMDA} and EPSC_{AMPA} were measured at $V_h = +40$ mV and $V_h = -40$ mV, respectively.

Table 2. Although most synaptic properties were indistinguishable in **P8-11** calyx of Held synapses of $Ca_v1.3^{-/-}$ compared to those of *wt* mice, AMPA EPSC amplitudes and probability of release were significantly different. Number of synapses tested is given in parenthesis. (n.s. = not significant; values are given as mean \pm SEM)

Parameter	<i>wt</i>	$Ca_v1.3^{-/-}$	
calyceal AP			
half-width (μ s)	331.3 \pm 13.6 (5)	338.4 \pm 26.9 (8)	n.s.
amplitude (mV)	132.7 \pm 1.3 (5)	133.9 \pm 3.1 (8)	n.s.
EPSC_{AMPA}			
amplitude (nA) ^a	5.02 \pm 0.40 (53)	6.84 \pm 0.64 (27)	p<0.05
CV	0.060 \pm 0.008	0.077 \pm 0.019	n.s.
rise time (20-80%) (ms) ^b	0.23 \pm 0.01 (14)	0.20 \pm 0.01 (9)	n.s.
decay ^b			
τ_{fast} (ms)	0.82 \pm 0.10 (13)	0.74 \pm 0.10 (9)	n.s.
τ_{slow} (ms)	4.50 \pm 0.64 (13)	4.28 \pm 0.89 (9)	n.s.
a_{fast} (%) ^c	78.7 \pm 1.3 (13)	80.8 \pm 2.1 (9)	n.s.
weighted τ_m (ms) ^d	1.50 \pm 0.21 (13)	1.33 \pm 0.30 (9)	n.s.
recovery time constant (s) ^e	3.9 \pm 0.3 (8)	3.46 \pm 0.4 (6)	n.s.
mEPSC			
frequency (s ⁻¹)	11 \pm 3 (8)	14 \pm 3 (8)	n.s.
amplitude (pA)	32.1 \pm 0.1 (8)	35.9 \pm 0.2 (8)	n.s.
rise time (20-80%) (μ s)	92.2 \pm 4.6 (8)	96.1 \pm 5.6 (8)	n.s.
decay time constant (ms)			
τ_{fast}	0.26 \pm 0.02 (8)	0.32 \pm 0.02 (8)	n.s.
τ_{slow}	1.44 \pm 0.19 (8)	2.03 \pm 0.50 (8)	n.s.
a_{fast} (%) ^c	84.9 \pm 1.5 (8)	88.3 \pm 1.8 (8)	n.s.
weighted τ_m (ms) ^d	0.44 \pm 0.05 (8)	0.50 \pm 0.05 (8)	n.s.
Quantal parameters			
F ^f	0.56 \pm 0.03 (35)	0.72 \pm 0.04 (13)	p<0.05
RRP ^f	628 \pm 66 (35)	577 \pm 55 (13)	n.s.
EPSC_{NMDA}			
amplitude (nA) ^g	6.34 \pm 0.44 (52)	5.52 \pm 0.46 (17)	n.s.
decay time constant (ms) ^g	72.0 \pm 3.6 (52)	84.9 \pm 4.8 (17)	n.s.
EPSC _{NMDA} /EPSC _{AMPA} ^h	1.29 \pm 0.08 (41)	0.75 \pm 0.06 (17)	p<0.001
ifenprodil block (%)	30.6 \pm 2.2 (18)	29.5 \pm 9.0 (4)	n.s.

^a Measured at $V_h = -40$ mV; ^b measured at $V_h = -70$ mV; ^c Relative amplitude of the fast decay component; ^d weighted mean decay time constant $\tau_m = a_{fast} * \tau_{fast} + a_{slow} * \tau_{slow}$, where a_{fast} and a_{slow} are the relative amplitudes of the fast and slow decay components, respectively; ^e time course of recovery from depression was estimated using conditioning 100 Hz trains; ^f estimated from synaptic depression during 100 Hz trains (Taschenberger et al., 2002); ^g measured at $V_h = +40$ mV; ^h EPSC_{NMDA} and EPSC_{AMPA} were measured at $V_h = +40$ mV and $V_h = -40$ mV, respectively.

4 DISCUSSION

The principle aim of this study was to compare the *in-vivo* maturation of a large glutamatergic CNS synapse, the calyx of Held, developing in the presence of normal (*wt* mice) or greatly reduced ($Ca_V1.3^{-/-}$ mice) levels of physiological afferent nerve activity. Such comparison allowed us to identify if previously described developmental changes in the functional properties of this synapse arise from intrinsic maturation processes or whether they are driven by afferent nerve activity.

We choose the $Ca_V1.3^{-/-}$ mouse model to address this question because: (1) $Ca_V1.3^{-/-}$ mice are deaf due to a complete absence of L-type Ca^{2+} currents in cochlear IHCs (Platzer et al., 2000; Brandt et al., 2003). (2) On the level of light microscopy, the morphology of IHCs and spiral ganglion cells seems to be preserved at least up to P14 and no gross disturbances in vestibular function and structure were found up to P35 (Platzer et al., 2000; Dou et al., 2004). (3) Glutamate release at later synapses along the auditory pathways is triggered by N-, P/Q-, and R-type Ca^{2+} channels (Iwasaki and Takahashi, 1998; Wu et al., 1998; Oleskevich and Walmsley, 2002) and does not rely on the expression of the L-type $Ca_V1.3$ subunit (Fig.6).

Our main findings of the analysis of presynaptic properties and synaptic transmission in $Ca_V1.3^{-/-}$ mice indicate similar properties of the exocytotic machinery but enhanced synaptic strength due to an elevated release probability and a delayed down regulation of synaptic NMDARs.

A straightforward approach to gain insight into the role of physiological nerve activity in regulating transmission at the calyx of Held synapses is to silence all auditory nerve input by cochlear ablation (Futai et al., 2001). However this approach suffers from the limitations that cochlear removal in young animals induces extensive axonal rewiring and a variety of trans-neuronal degenerative effects within the auditory brainstem (Hashisaki and Rubel, 1989; Russell and Moore, 1995). We therefore choose a different approach by making use of the fact that Ca^{2+} channels governing transmitter release in IHCs are distinct from those found at higher synapses along the auditory pathways.

We compared transmission at calyx of Held synapses in *wt* and *Ca_v1.3^{-/-}* mice assuming that the latter develop in the presence of greatly reduced levels of afferent nerve activity. Is this assumption justified?

Sound-evoked auditory brainstem responses are missing in *Ca_v1.3^{-/-}* mice (Platzer et al., 2000). However, some neurons of the ventral cochlear nucleus exhibit high spontaneous discharge rates even in the absence of sound. Average spontaneous discharge frequencies correlate with the characteristic frequency of the respective cells (Pfeiffer and Kiang, 1965; Friauf and Ostwald, 1988; Smith et al., 1991; Kopp-Scheinflug et al., 2003).

It is not certain whether intact transmission at the IHC-spiral neuron synapse is absolutely required for spontaneous activity at the level of the VCN. However, most of it appears to be cochlea-driven because almost all activity in the VCN disappears immediately after cochlear destruction (Koerber et al., 1966). Very little is known about spontaneous activity in the rodent auditory pathway before hearing onset. At this age, cochlear IHCs spontaneously generate Ca^{2+} APs (Kros et al., 1998; Glowatzki and Fuchs, 2000) which trigger glutamate release

(Beutner and Moser, 2001) and possibly AP firing in the auditory nerve. Since sound-evoked activity as well as spontaneous activity before hearing onset and possibly also thereafter rely on intact glutamate release from cochlear IHCs, it is highly likely that the levels of afferent nerve activity as well as their temporal pattern differ greatly between calyx of Held synapses of *wt* and *Ca_v1.3^{-/-}* mice.

4.1 Synaptic transmission is intact in mature *Ca_v1.3^{-/-}* calyx of Held-MNTB synapses

The large size of the calyx of Held allows it to harbor hundreds of active zones and thus a single presynaptic AP releases hundreds of quanta, generating a large EPSC that rapidly depolarizes the MNTB neuron to firing threshold (Fig. 4A,B). In addition to the calyceal input, principal cells receive also conventional excitatory and inhibitory synapses (Forsythe and Barnes-Davies, 1993a; Hamann et al., 2003), which may generate small EPSPs and IPSPs in MNTB neurons (Fig. 4C). In some recordings we observed that small EPSPs can depolarize the MNTB principal neuron close to firing threshold and occasionally even trigger postsynaptic APs (Fig. 4A, arrows), in addition to the one evoked by the calyx of Held. During trains of afferent fiber stimulation, EPSC depression (due to vesicle pool depletion or desensitization of postsynaptic AMPA receptors) translates into depression of EPSPs. The latter effect causes variability in the time at which AP threshold is reached, producing jitter in the timing of action potential firing (Chuhma and Ohmori, 1998; Taschenberger and von Gersdorff, 2000; Brenowitz and Trussell, 2001). At 20 Hz stimulation, we observed a mild effect of these phenomena in *Ca_v1.3^{-/-}* mice (Fig. 4A, right panel).

We then asked how reliably $Ca_v1.3^{-/-}$ calyces would respond to high-frequency stimulation, i.e. if they would fire an AP per each stimulus given. No significant differences in presynaptic AP failures were found in $Ca_v1.3^{-/-}$ compared to *wt* terminals (Fig. 5). These results suggest that the mechanisms of basal synaptic transmission are unchanged in $Ca_v1.3^{-/-}$ mice and that $Ca_v1.3^{-/-}$ calyces are as reliable as *wt* presynaptic terminals.

4.2 Developmental refinement of presynaptic properties in the absence of afferent nerve activity

Our data indicate that some developmental refinement of presynaptic properties occurs irrespective of the presence or absence of cochlea-driven nerve activity. In P14-17 terminals for example, calyceal APs in both *wt* and $Ca_v1.3^{-/-}$ mice were significantly faster than those recorded in younger mice (Fedchyshyn and Wang, 2005) and rats (Taschenberger and von Gersdorff, 2000).

In developing rat calyces, the amplitude of $I_{Ca(V)}$ increases and Ca^{2+} channels differ between immature and mature calyces not only regarding their subtypes (Iwasaki and Takahashi, 1998) but probably also in their spatial distribution relative to the release sites. The removal of distant Ca^{2+} channels (Fedchyshyn and Wang, 2005) probably results in a more efficient exocytosis ($\Delta C_m/Q_{Ca}$) by a factor of ~ 1.6 from P5 to P14 (Taschenberger et al., 2002). Evidence obtained from EM analysis as well as presynaptic C_m recordings and analysis of synaptic depression during high-frequency trains at various stages of development further suggest that the *RRP* increases in the rat calyx of Held (Iwasaki and Takahashi, 2001; Meyer et al., 2001; Satzler et al., 2002; Taschenberger et al., 2002).

In the present study, presynaptic Ca^{2+} currents were indistinguishable between *wt* and *Ca_v1.3^{-/-}* mice at P14-17 (Fig. 6). Moreover, neither $\Delta C_m/Q_{\text{Ca}}$ ratios nor *RRP* size estimates based on amplitudes of capacitance jumps (Fig. 7) or eEPSC recordings (Fig. 14 and Table 1) were different between *wt* and *Ca_v1.3^{-/-}* mice at this age.

Considering its extensive developmental refinement it seems surprising that the presynaptic release machinery of the calyx terminal is rather robust and many functional properties are little affected by chronic changes of activity levels.

4.3 The level of afferent nerve activity regulates release probability

Using a similar approach as applied before to the neuromuscular junction (Elmqvist and Quastel, 1965; Christensen and Martin, 1970) we estimate that *F* drops from 0.56 to 0.31 in *wt* and from 0.72 to 0.50 in *Ca_v1.3^{-/-}* mice (Fig. 14). These values are comparable to estimates based on measured *PPRs* (Fig. 12) which also indicated a decreasing *F*. A relatively low release fraction in P14-17 calyx synapses is further suggested by presynaptic ΔC_m recordings which showed that single AP-like depolarizations released only a small fraction of the available vesicles (Fig. 7).

These results are similar to those previously published at the rat calyx of Held (Iwasaki and Takahashi, 2001; Taschenberger et al., 2002) and other central glutamatergic synapses (Muller et al., 1989; Bolshakov and Siegelbaum, 1995; Reyes and Sakmann, 1999; Brenowitz and Trussell, 2001). These studies also showed a decreasing release probability during postnatal development. In contrast, relatively high release probability was recently reported for P12

calyces of mice (Oleskevich et al., 2004; Youssoufian et al., 2005). However, the experimentally measured average eEPSC amplitudes in those studies are difficult to reconcile with the product Npq using their estimates for the respective quantities.

A key conclusion in this study is that, regardless of the method applied to determine F , we always estimated its value to be higher in $Ca_v1.3^{-/-}$ compared with wt mice. Interestingly, this also holds for P8-11 synapses (Table 2) suggesting a possible role of cochlea-driven spontaneous nerve activity in regulating F . Another alternative explanation is that differences may arise at this age because some P11 pups already could experience evoked auditory activity. The latter would accentuate a difference in F due to a decrease of release probability driven by afferent activity in P11 wt synapses.

We then asked for the underlying mechanism of a higher release probability in $Ca_v1.3^{-/-}$ synapses. Presynaptically, modulation of the release probability during development may be mediated by changes in AP waveform, Ca^{2+} channel conductance and/or Ca^{2+} channel number, Ca^{2+} ions sensitivity of the Ca^{2+} sensor coupled to vesicle fusion, and extrusion and/or equilibrium of Ca^{2+} by presynaptic Ca^{2+} buffers. Here, we report no differences in presynaptic Ca^{2+} currents amplitude and facilitation, or in the efficiency of Ca^{2+} -mediated vesicle exocytosis. Thus, our results suggest that Ca^{2+} channel population and the machinery of release coupled to Ca^{2+} influx are unchanged in $Ca_v1.3^{-/-}$ compared to wt terminals.

An unexpected finding of this study was the slower presynaptic AP waveform in $Ca_v1.3^{-/-}$ compared with wt mice (Fig. 8). During normal development, calyceal APs exhibit a shortening in their half widths from around 400 μs to 200 μs before and after the onset of hearing (P12-13), respectively (Taschenberger

and von Gersdorff, 2000; Taschenberger et al., 2002; Dodson et al., 2003). Our observations suggest that in presynaptic terminals developing in the absence of evoked afferent activity, this acceleration in the AP time-course is not complete as compared to *wt* mice.

This difference may be linked to changes in the expression or modulation of voltage-gated K⁺ channels of the K_v3 type. These channels are generally associated with high frequency AP firing and mediate rapid spike repolarization in many areas of the CNS (Rudy and McBain, 2001). Furthermore, it has been shown that blocking K_v3 currents with low concentrations (1-3 mM) of tetraethylammonium (TEA) increases AP duration (Wang and Kaczmarek, 1998).

Previous studies showed that activity-dependent changes in K_v3 channel activity are mediated by channel phosphorylation by casein kinase II (Macica and Kaczmarek, 2001) and protein kinase C (Macica et al., 2003). In MNTB neurons, there is a high basal phosphorylation at ser503 of Kv3.1b decreasing the postsynaptic K⁺-current amplitude. Interestingly, high-frequency acoustic stimulation can rapidly modulate the firing pattern of these postsynaptic cells by dephosphorylating voltage-gated K⁺ channels (Song et al., 2005). And given the broad distribution of phosphorylated- Kv3.1b in both postsynaptic and presynaptic compartments of the calyx of Held-MNTB synapse (Song et al., 2005), Kv3.1b modulation may also occur in the presynaptic terminal. Moreover, another study reported that the tonotopic organization of MNTB principal neurons with respect to their expression of voltage-gated K⁺ channels is disrupted in congenitally deaf mice (Leao et al., 2006). This observation further supports the idea that voltage-gated K⁺ channel expression could be regulated by afferent nerve activity.

In conclusion, our results suggest that the presynaptic AP time-course is regulated, at least in part, by afferent activity during development. Thus, based on previous evidence obtained in rat calyces (Borst and Sakmann, 1998a, 1999; Taschenberger and von Gersdorff, 2000), our own modeling (Fig. 8) and because of the similar Ca^{2+} influx (Fig.6) and $\Delta C_m/Q_{\text{Ca}}$ ratios (Fig. 7), we consider it likely that the difference in presynaptic AP waveform between *wt* and *Ca_v1.3^{-/-}* mice represents the main mechanism underlying the higher release probability in the latter.

A wider AP waveform will increase the amount of Ca^{2+} ions that will flow into the presynaptic terminal. In the present study, an augmented presynaptic Ca^{2+} influx is further suggested by an increased asynchronous release rate after train stimulation in *Ca_v1.3^{-/-}* mice (Fig. 11B). Previous studies have shown that asynchronous release is primarily related to the build up of intracellular Ca^{2+} during repetitive stimulation. For instance, asynchronous release rates in response to trains of action potentials are reduced by the application of calcium buffers at the calyx synapse (Chuhma et al., 2001; Oleskevich and Walmsley, 2002) and in hippocampal cultures (Hagler and Goda, 2001; Otsu et al., 2004). The latter supports the idea that elevated presynaptic Ca^{2+} transients would lead to a higher number of delayed miniature events.

Likewise, the replenishment of synaptic vesicles after high frequency stimulation is accelerated in the presence of high intracellular Ca^{2+} concentration. Our results showed an accelerated recovery from depression in *Ca_v1.3^{-/-}* mice (Fig. 13, Table 1), consistent with wider presynaptic APs leading to an elevated intraterminal Ca^{2+} concentration. Interestingly, Wang and Kaczmarek (1998) reported that vesicle turnover was faster after application of the K^+ channel

blocker TEA, which widens presynaptic action potential waveform and thus increases Ca^{2+} influx. The authors concluded that elevated Ca^{2+} entry during repetitive firing of action potentials is the key element that enhances the replenishment.

In conclusion, our results showing a higher asynchronous release rate (Fig. 11) and a faster vesicle replenishment (Fig. 13), further support the finding of wider presynaptic APs leading to an increased Ca^{2+} influx in $\text{Ca}_v1.3^{-/-}$ synapses

Presynaptic mechanisms responsible for an up-regulation of synaptic strength in response to synaptic disuse have been described for other auditory synapses before. At endbulb synapses of the mouse VCN, release probability and a higher asynchronous release rate are increased after chronic reduction in activity levels (Oleskevich and Walmsley, 2002). Our study is in close agreement with the latter work, which also suggests a higher intracellular Ca^{2+} concentration in endbulb calyces of deaf mice. Oleskevich et al. (2002) proposed that endogenous calcium buffering may be impaired or underdeveloped in presynaptic terminals of deaf mice, as the difference in release probability can be reversed by the addition of EGTA-AM (a membrane permeable intracellular calcium buffer) (Oleskevich and Walmsley, 2002). However, since presynaptic properties were not directly measured at endbulb calyces, the underlying mechanism for a higher release probability remains unclear in the VCN of deaf mouse. It is possible that a similar effect of wider APs leading to higher Ca^{2+} influx may occur at the endbulb presynaptic terminals, accounting at least in part, for the increased vesicle release probability.

On the other hand, previous studies using congenitally deaf mice demonstrated

that the development of synaptic strength is not affected by auditory nerve activity at the calyx of Held-MNTB synapse (Oleskevich et al., 2004; Youssoufian et al., 2005). One explanation for the conflicting results with the present study is the age window when the measurements were made (until P14 or even earlier). In contrast, we recorded properties of pre- and postsynaptic transmission until 17 days after birth, considerably after the onset of hearing period (P12-13).

4.4 Postsynaptic AMPA and NMDA receptors show different sensitivity to chronic changes in afferent nerve activity

4.4.1 AMPA receptors are not affected by reduced levels of activity

The strengthening of AMPA transmission at calyx synapses developing in the absence of cochlea-driven nerve activity was mainly due to increased glutamate release. In *Ca_v1.3^{-/-}* mice, AMPA-receptor mediated EPSCs were on average 54% larger than in *wt* animals (Fig. 9). This result is in close agreement to the relative increase in eEPSC amplitudes predicted from measured presynaptic APs (see results, Fig. 8). This similarity further supports the idea that EPSC_{AMPA} is larger in *Ca_v1.3^{-/-}* mice due to a presynaptic change in AP waveform.

Amplitudes of mEPSCs were unaffected by the lack of afferent nerve activity during development (Fig 10). Moreover, we observed a similar developmental acceleration of mEPSC and eEPSC decay kinetics in *wt* and *Ca_v1.3^{-/-}* mice. Assuming that these changes reflect differences in AMPAR subunit composition (Joshi et al., 2004) we may conclude that at the calyx of Held, the developmental regulation of postsynaptic AMPAR expression is largely unaffected by the level of afferent nerve activity.

4.4.2 NMDA receptors are regulated by afferent nerve activity

A common feature of many forms of synaptic plasticity is an alteration in the number or complement of NMDA-type glutamate receptors (Rao and Craig, 1997; Quinlan et al., 1999b; Watt et al., 2000). The present study shows that, in contrast to the developmental profile of AMPARs in deaf animals, the down regulation and the developmental switch in subunit expression for synaptic NMDARs seems to be at least partly activity-dependent because it is delayed in the absence of cochlea-driven nerve activity (Fig. 17).

Recent studies at central glutamatergic synapses have shown that, activity-dependent alterations in NMDA receptor trafficking, may account for changes in number and subunit composition of NMDA-receptors (Perez-Otano and Ehlers, 2005). For example, it has been suggested that visual experience, olfactory learning and auditory activity increase the proportion of NR2A-containing receptors at central synapses (Quinlan et al., 1999a; Quinlan et al., 1999b; Futai et al., 2001) and thus shortens the duration of NMDAR currents (Flint et al., 1997; Stocca and Vicini, 1998). Conversely, visual deprivation and deafness slow or reverse the switch from NR2B to NR2A (Futai et al., 2001; Philpot et al., 2001). One explanation for the latter findings may be that, although synaptic insertion of NR2B-containing receptors is constitutive and does not require synaptic activity, their replacement by NR2A-containing receptors is use dependent (Barria and Malinow, 2002).

Interestingly, activity also alters the expression of scaffolding proteins that provide anchors for these receptors. For instance, the levels of PSD-95, which preferentially binds NR2A subunits, are regulated during development (Sans et al., 2000), and experience rapidly increases dendritic PSD-95 expression in visual pathways (Townsend et al., 2003).

Our results compare well to those obtained in the above mentioned studies using different model synapses, suggesting that NMDA receptor expression and composition are generally regulated by nerve activity. However, the mechanisms by which these modifications occur at the calyx of Held synapse remain to be clarified. On the other hand, the beginning decrease of NMDAR subunit proteins before onset of hearing suggest the involvement of additional regulatory mechanisms, distinct to afferent nerve activity (Futai et al., 2001).

4.5 Comparison to in vitro studies

Our observations from mice developing in the absence of auditory activity, suggested changes in presynaptic AP waveform as well as postsynaptic delayed down regulation and subunit switching of NMDA receptors. During maturation of MNTB neurons, we did not detect modifications in the number or composition of AMPAR, suggesting that presynaptic and postsynaptic properties are not homogeneously affected by the lack of cochlea-driven activity. In this section we compare our results with several proposed mechanisms underlying homeostatic plasticity in cultured cortical neurons (Turrigiano and Nelson, 2004).

Upon pharmacological silencing using TTX, cultured glutamatergic hippocampal synapses responded with an upregulation of the RRP size together with an increase in synapse dimensions (Murthy et al., 2001). The latter study indicates that changes in presynaptic properties contribute to homeostatic synaptic plasticity in central neurons. The authors showed that active zone size and the number of docked vesicles per active zone are increased after 2-5 days of activity blockade. In addition, the size of the recycling vesicle pool is also increased during chronic TTX application. In contrast, our results provided no

evidence for an increased RRP but suggested an elevated release probability.

On the other hand, silencing synaptic activity in cultured cortical networks with TTX or glutamate receptor antagonists resulted in larger quantal amplitudes (Turrigiano et al., 1998; Leslie et al., 2001). For the calyx of Held such rule does not seem to apply because AMPA mEPSCs increased similarly in amplitude during development in both *wt* and *Ca_v1.3^{-/-}* mice (Fig. 10).

Discrepancies with our study may be further accentuated because our model is at the single synapse level; each postsynaptic cell receives only one large presynaptic input. Thus, fluctuations in the level of afferent activity will only affect a unitary synaptic connection. For cultured hippocampal neurons or cortical neuronal networks *in vivo*, the problem is much more complex. These neurons integrate connections from hundreds or thousands of presynaptic inputs and form an intricate system that may be regulated differently depending on how activity is modulated (blocked or enhanced).

For instance, AMPAR blockade in hippocampal cultures during postnatal development increases both the frequency and amplitude of mEPSCs (Thiagarajan et al., 2002). In contrast, lowering activity in individual hippocampal neurons by expression of an inward rectifier (K_{ir}) potassium channel produced a small increase in mEPSC frequency but no change in amplitude (Burrone et al., 2002). These examples further suggest that the compensatory mechanisms activated by lowering activity in individual neurons are distinct from those engaged by lowering network activity (Turrigiano and Nelson, 2004).

In addition, the locus of expression (whether it is presynaptic or postsynaptic) of homeostatic plasticity seems to depend on different developmental stages

(Wierenga et al., 2006). Moreover, many forms of cortical plasticity have critical periods during which sensory experience can alter circuit properties, but outside of which sensory experience has little or no effect (Turrigiano and Nelson, 2004). For example, synaptic scaling in the visual cortex is developmentally regulated. Two days of monocular deprivation beginning at P14 (immediately before eye opening) scales up mEPSC amplitudes onto principle neurons (star pyramids) in layer 4, but the same treatment has no effect when begun at P21. By contrast, mEPSC onto layer 2/3 pyramidal neurons were unaffected by monocular deprivation beginning at P14, but were scaled up by monocular deprivation beginning at P21 (Guire et al., 1999). These data indicate that the sites of homeostatic plasticity could migrate to different cortical layers in an age-dependent manner. These critical periods may also apply to changes in synaptic strength at the individual synapse level. The opposing results between our study ($Ca_v1.3^{-/-}$, P8-P17) and using congenitally deaf mutant mice (dn/dn) as a model (Oleskevich et al., 2004; Youssoufian et al., 2005), suggest that the site for homeostatic plasticity in the auditory pathway may also shift in an age-dependent manner.

We conclude that different rules may apply for homeostatic regulation of synaptic strength at different glutamatergic synapses. These rules seem to depend on the type of experimental preparation, the observed developmental stage and the means by which afferent nerve activity is suppressed.

This and other studies leave several open questions. For instance, how changes in activity are read out by the molecular machinery; and what intracellular signal transduction cascades generate global changes in synaptic strength. Even when the mechanisms that determine plasticity are more

sophisticated and diverse than previously thought, it would be of great insight to correlate these physiological findings to the cell biological and molecular level.

5 SUMMARY

We studied how afferent nerve activity affects the *in-vivo* maturation of a fast glutamatergic CNS synapse, the calyx of Held. To address this question we exploited the distinct presynaptic Ca^{2+} channel subtypes governing transmitter release at the cochlear inner hair cell (IHC)-spinal neuron synaptic junction compared to those at higher synapses along the auditory pathways. We characterized functional properties of calyx synapses in wildtype (*wt*) compared to those developing in *Ca_v1.3 subunit-deficient* ($\text{Ca}_v1.3^{-/-}$) mice. The latter are deaf because of absence of glutamate release from IHC and degeneration of primary afferents and thus completely lack cochlea-driven nerve activity. Ca^{2+} -channel properties, Ca^{2+} dependence of exocytosis, number of readily releasable quanta and AMPA mEPSCs were unchanged in P14-17 calyx synapses of $\text{Ca}_v1.3^{-/-}$ mice. However, synaptic strength was augmented because presynaptic action potentials were broader leading to increased quantal release, consistent with lower paired-pulse ratios and stronger depression during repetitive synaptic stimulation. Furthermore, asynchronous release following trains was elevated presumably because of higher residual Ca^{2+} accumulating in the presynaptic terminals. Finally, we measured larger NMDA EPSCs with higher sensitivity to the NR2B subunit-specific antagonist ifenprodil in P14-17 synapses of $\text{Ca}_v1.3^{-/-}$ compared to *wt* mice. These results suggest that auditory activity is required for the adjustment of synaptic strength as well as for the down regulation of synaptic NMDARs during postnatal development of the calyx of Held. In contrast, properties of the presynaptic release machinery and postsynaptic AMPARs are unaffected by chronic changes in the level of afferent activity at this synapse.

REFERENCES

- Bacci A, Coco S, Pravettoni E, Schenk U, Armano S, Frassoni C, Verderio C, De Camilli P, Matteoli M (2001) Chronic blockade of glutamate receptors enhances presynaptic release and downregulates the interaction between synaptophysin-synaptobrevin-vesicle-associated membrane protein 2. *J Neurosci* 21:6588-6596.
- Banks MI, Smith PH (1992) Intracellular recordings from neurobiotin-labeled cells in brain slices of the rat medial nucleus of the trapezoid body. *J Neurosci* 12:2819-2837.
- Barria A, Malinow R (2002) Subunit-specific NMDA receptor trafficking to synapses. *Neuron* 35:345-353.
- Beutner D, Moser T (2001) The presynaptic function of mouse cochlear inner hair cells during development of hearing. *J Neurosci* 21:4593-4599.
- Billups B, Forsythe ID (2002) Presynaptic mitochondrial calcium sequestration influences transmission at mammalian central synapses. *J Neurosci* 22:5840-5847.
- Bollmann JH, Sakmann B, Borst JG (2000) Calcium sensitivity of glutamate release in a calyx-type terminal. *Science* 289:953-957.
- Bolshakov VY, Siegelbaum SA (1995) Regulation of hippocampal transmitter release during development and long-term potentiation. *Science* 269:1730-1734.
- Borst JG, Sakmann B (1996) Calcium influx and transmitter release in a fast CNS synapse. *Nature* 383:431-434.
- Borst JG, Sakmann B (1998a) Calcium current during a single action potential in a large presynaptic terminal of the rat brainstem. *J Physiol* 506 (Pt 1):143-157.
- Borst JG, Sakmann B (1998b) Facilitation of presynaptic calcium currents in the rat brainstem. *J Physiol* 513 (Pt 1):149-155.
- Borst JG, Sakmann B (1999) Effect of changes in action potential shape on calcium currents and transmitter release in a calyx-type synapse of the rat auditory brainstem. *Philos Trans R Soc Lond B Biol Sci* 354:347-355.
- Borst JG, Helmchen F, Sakmann B (1995) Pre- and postsynaptic whole-cell recordings in the medial nucleus of the trapezoid body of the rat. *J Physiol* 489 (Pt 3):825-840.
- Brand A, Behrend O, Marquardt T, McAlpine D, Grothe B (2002) Precise inhibition is essential for microsecond interaural time difference coding. *Nature* 417:543-547.

- Brandt A, Striessnig J, Moser T (2003) CaV1.3 channels are essential for development and presynaptic activity of cochlear inner hair cells. *J Neurosci* 23:10832-10840.
- Brenowitz S, Trussell LO (2001) Maturation of synaptic transmission at end-bulb synapses of the cochlear nucleus. *J Neurosci* 21:9487-9498.
- Brew HM, Forsythe ID (1995) Two voltage-dependent K⁺ conductances with complementary functions in postsynaptic integration at a central auditory synapse. *J Neurosci* 15:8011-8022.
- Burrone J, Murthy VN (2003) Synaptic gain control and homeostasis. *Curr Opin Neurobiol* 13:560-567.
- Burrone J, O'Byrne M, Murthy VN (2002) Multiple forms of synaptic plasticity triggered by selective suppression of activity in individual neurons. *Nature* 420:414-418.
- Chattopadhyaya B, Di Cristo G, Higashiyama H, Knott GW, Kuhlman SJ, Welker E, Huang ZJ (2004) Experience and activity-dependent maturation of perisomatic GABAergic innervation in primary visual cortex during a postnatal critical period. *J Neurosci* 24:9598-9611.
- Christensen BN, Martin AR (1970) Estimates of probability of transmitter release at the mammalian neuromuscular junction. *J Physiol* 210:933-945.
- Chuhma N, Ohmori H (1998) Postnatal development of phase-locked high-fidelity synaptic transmission in the medial nucleus of the trapezoid body of the rat. *J Neurosci* 18:512-520.
- Chuhma N, Koyano K, Ohmori H (2001) Synchronisation of neurotransmitter release during postnatal development in a calyceal presynaptic terminal of rat. *J Physiol* 530:93-104.
- Clem RL, Barth A (2006) Pathway-specific trafficking of native AMPARs by in vivo experience. *Neuron* 49:663-670.
- Clements JD (1990) A statistical test for demonstrating a presynaptic site of action for a modulator of synaptic amplitude. *J Neurosci Methods* 31:75-88.
- Clements JD, Bekkers JM (1997) Detection of spontaneous synaptic events with an optimally scaled template. *Biophys J* 73:220-229.
- Cuttle MF, Tsujimoto T, Forsythe ID, Takahashi T (1998) Facilitation of the presynaptic calcium current at an auditory synapse in rat brainstem. *J Physiol* 512 (Pt 3):723-729.
- de Lange RP, de Roos AD, Borst JG (2003) Two modes of vesicle recycling in the rat calyx of Held. *J Neurosci* 23:10164-10173.

- Debanne D, Guerineau NC, Gähwiler BH, Thompson SM (1996) Paired-pulse facilitation and depression at unitary synapses in rat hippocampus: quantal fluctuation affects subsequent release. *J Physiol* 491 (Pt 1):163-176.
- Desai NS, Rutherford LC, Turrigiano GG (1999) Plasticity in the intrinsic excitability of cortical pyramidal neurons. *Nat Neurosci* 2:515-520.
- Diamond JS, Jahr CE (1995) Asynchronous release of synaptic vesicles determines the time course of the AMPA receptor-mediated EPSC. *Neuron* 15:1097-1107.
- Dobrunz LE, Stevens CF (1997) Heterogeneity of release probability, facilitation, and depletion at central synapses. *Neuron* 18:995-1008.
- Dodson PD, Billups B, Rusznak Z, Szucs G, Barker MC, Forsythe ID (2003) Presynaptic rat Kv1.2 channels suppress synaptic terminal hyperexcitability following action potential invasion. *J Physiol* 550:27-33.
- Dou H, Vazquez AE, Namkung Y, Chu H, Cardell EL, Nie L, Parson S, Shin HS, Yamoah EN (2004) Null mutation of alpha1D Ca²⁺ channel gene results in deafness but no vestibular defect in mice. *J Assoc Res Otolaryngol* 5:215-226.
- Ehlers MD (2000) Reinsertion or degradation of AMPA receptors determined by activity-dependent endocytic sorting. *Neuron* 28:511-525.
- Elmqvist D, Quastel DM (1965) A quantitative study of end-plate potentials in isolated human muscle. *J Physiol* 178:505-529.
- Faber DS, Korn H (1991) Applicability of the coefficient of variation method for analyzing synaptic plasticity. *Biophys J* 60:1288-1294.
- Fedchyshyn MJ, Wang LY (2005) Developmental transformation of the release modality at the calyx of held synapse. *J Neurosci* 25:4131-4140.
- Flint AC, Maisch US, Weishaupt JH, Kriegstein AR, Monyer H (1997) NR2A subunit expression shortens NMDA receptor synaptic currents in developing neocortex. *J Neurosci* 17:2469-2476.
- Forsythe ID (1994) Direct patch recording from identified presynaptic terminals mediating glutamatergic EPSCs in the rat CNS, in vitro. *J Physiol* 479 (Pt 3):381-387.
- Forsythe ID, Barnes-Davies M (1993a) The binaural auditory pathway: excitatory amino acid receptors mediate dual timecourse excitatory postsynaptic currents in the rat medial nucleus of the trapezoid body. *Proc Biol Sci* 251:151-157.
- Forsythe ID, Barnes-Davies M (1993b) The binaural auditory pathway: membrane currents limiting multiple action potential generation in the rat medial nucleus of the trapezoid body. *Proc Biol Sci* 251:143-150.

- Friauf E, Ostwald J (1988) Divergent projections of physiologically characterized rat ventral cochlear nucleus neurons as shown by intra-axonal injection of horseradish peroxidase. *Exp Brain Res* 73:263-284.
- Futai K, Okada M, Matsuyama K, Takahashi T (2001) High-fidelity transmission acquired via a developmental decrease in NMDA receptor expression at an auditory synapse. *J Neurosci* 21:3342-3349.
- Geiger JR, Melcher T, Koh DS, Sakmann B, Seeburg PH, Jonas P, Monyer H (1995) Relative abundance of subunit mRNAs determines gating and Ca²⁺ permeability of AMPA receptors in principal neurons and interneurons in rat CNS. *Neuron* 15:193-204.
- Glowatzki E, Fuchs PA (2000) Cholinergic synaptic inhibition of inner hair cells in the neonatal mammalian cochlea. *Science* 288:2366-2368.
- Guire ES, Lickey ME, Gordon B (1999) Critical period for the monocular deprivation effect in rats: assessment with sweep visually evoked potentials. *J Neurophysiol* 81:121-128.
- Hagler DJ, Jr., Goda Y (2001) Properties of synchronous and asynchronous release during pulse train depression in cultured hippocampal neurons. *J Neurophysiol* 85:2324-2334.
- Hamann M, Billups B, Forsythe ID (2003) Non-calyceal excitatory inputs mediate low fidelity synaptic transmission in rat auditory brainstem slices. *Eur J Neurosci* 18:2899-2902.
- Hashisaki GT, Rubel EW (1989) Effects of unilateral cochlea removal on anteroventral cochlear nucleus neurons in developing gerbils. *J Comp Neurol* 283:465-473.
- Hefft S, Jonas P (2005) Asynchronous GABA release generates long-lasting inhibition at a hippocampal interneuron-principal neuron synapse. *Nat Neurosci* 8:1319-1328.
- Helmchen F, Borst JG, Sakmann B (1997) Calcium dynamics associated with a single action potential in a CNS presynaptic terminal. *Biophys J* 72:1458-1471.
- Hessler NA, Shirke AM, Malinow R (1993) The probability of transmitter release at a mammalian central synapse. *Nature* 366:569-572.
- Hoffpauir BK, Grimes JL, Mathers PH, Spirou GA (2006) Synaptogenesis of the calyx of Held: rapid onset of function and one-to-one morphological innervation. *J Neurosci* 26:5511-5523.
- Inchauspe CG, Martini FJ, Forsythe ID, Uchitel OD (2004) Functional compensation of P/Q by N-type channels blocks short-term plasticity at the calyx of held presynaptic terminal. *J Neurosci* 24:10379-10383.

- Ishikawa T, Kaneko M, Shin HS, Takahashi T (2005) Presynaptic N-type and P/Q-type Ca²⁺ channels mediating synaptic transmission at the calyx of Held of mice. *J Physiol* 568:199-209.
- Iwasaki S, Takahashi T (1998) Developmental changes in calcium channel types mediating synaptic transmission in rat auditory brainstem. *J Physiol* 509 (Pt 2):419-423.
- Iwasaki S, Takahashi T (2001) Developmental regulation of transmitter release at the calyx of Held in rat auditory brainstem. *J Physiol* 534:861-871.
- Iwasaki S, Momiyama A, Uchitel OD, Takahashi T (2000) Developmental changes in calcium channel types mediating central synaptic transmission. *J Neurosci* 20:59-65.
- Jonas P, Major G, Sakmann B (1993) Quantal components of unitary EPSCs at the mossy fibre synapse on CA3 pyramidal cells of rat hippocampus. *J Physiol* 472:615-663.
- Joris PX, Smith PH, Yin TC (1998) Coincidence detection in the auditory system: 50 years after Jeffress. *Neuron* 21:1235-1238.
- Joshi I, Wang LY (2002) Developmental profiles of glutamate receptors and synaptic transmission at a single synapse in the mouse auditory brainstem. *J Physiol* 540:861-873.
- Joshi I, Shokralla S, Titis P, Wang LY (2004) The role of AMPA receptor gating in the development of high-fidelity neurotransmission at the calyx of Held synapse. *J Neurosci* 24:183-196.
- Kandler K, Friauf E (1993) Pre- and postnatal development of efferent connections of the cochlear nucleus in the rat. *J Comp Neurol* 328:161-184.
- Katz B (1969) The release of neural transmitter substances. Liverpool, England: Liverpool University Press.
- Kikuchi K, Hilding D (1965) The development of the organ of Corti in the mouse. *Acta Otolaryngol* 60:207-222.
- Kirov SA, Harris KM (1999) Dendrites are more spiny on mature hippocampal neurons when synapses are inactivated. *Nat Neurosci* 2:878-883.
- Koerber KC, Pfeiffer RR, Warr WB, Kiang NY (1966) Spontaneous spike discharges from single units in the cochlear nucleus after destruction of the cochlea. *Exp Neurol* 16:119-130.
- Koike-Tani M, Saitoh N, Takahashi T (2005) Mechanisms underlying developmental speeding in AMPA-EPSC decay time at the calyx of Held. *J Neurosci* 25:199-207.

- Kopp-Scheinflug C, Fuchs K, Lippe WR, Tempel BL, Rubsamen R (2003) Decreased temporal precision of auditory signaling in *Kcna1*-null mice: an electrophysiological study in vivo. *J Neurosci* 23:9199-9207.
- Kros CJ, Ruppersberg JP, Rusch A (1998) Expression of a potassium current in inner hair cells during development of hearing in mice. *Nature* 394:281-284.
- Kuwabara N, DiCaprio RA, Zook JM (1991) Afferents to the medial nucleus of the trapezoid body and their collateral projections. *J Comp Neurol* 314:684-706.
- Leao RM, Kushmerick C, Pinaud R, Renden R, Li GL, Taschenberger H, Spirou G, Levinson SR, von Gersdorff H (2005) Presynaptic Na⁺ channels: locus, development, and recovery from inactivation at a high-fidelity synapse. *J Neurosci* 25:3724-3738.
- Leao RN, Sun H, Svahn K, Berntson A, Yousoufian M, Paolini AG, Fyffe RE, Walmsley B (2006) Topographic organization in the auditory brainstem of juvenile mice is disrupted in congenital deafness. *J Physiol* 571:563-578.
- Leslie KR, Nelson SB, Turrigiano GG (2001) Postsynaptic depolarization scales quantal amplitude in cortical pyramidal neurons. *J Neurosci* 21:RC170.
- Lindlbauer R, Mohrmann R, Hatt H, Gottmann K (1998) Regulation of kinetic and pharmacological properties of synaptic NMDA receptors depends on presynaptic exocytosis in rat hippocampal neurones. *J Physiol* 508 (Pt 2):495-502.
- Liu XB, Murray KD, Jones EG (2004) Switching of NMDA receptor 2A and 2B subunits at thalamic and cortical synapses during early postnatal development. *J Neurosci* 24:8885-8895.
- Llinas R, Steinberg IZ, Walton K (1981) Relationship between presynaptic calcium current and postsynaptic potential in squid giant synapse. *Biophys J* 33:323-351.
- Macica CM, Kaczmarek LK (2001) Casein kinase 2 determines the voltage dependence of the Kv3.1 channel in auditory neurons and transfected cells. *J Neurosci* 21:1160-1168.
- Macica CM, von Hehn CA, Wang LY, Ho CS, Yokoyama S, Joho RH, Kaczmarek LK (2003) Modulation of the kv3.1b potassium channel isoform adjusts the fidelity of the firing pattern of auditory neurons. *J Neurosci* 23:1133-1141.
- Marty S, Wehrle R, Sotelo C (2000) Neuronal activity and brain-derived neurotrophic factor regulate the density of inhibitory synapses in organotypic slice cultures of postnatal hippocampus. *J Neurosci* 20:8087-8095.

- Meinrenken CJ, Borst JG, Sakmann B (2003) Local routes revisited: the space and time dependence of the Ca^{2+} signal for phasic transmitter release at the rat calyx of Held. *J Physiol* 547:665-689.
- Meyer AC, Neher E, Schneggenburger R (2001) Estimation of quantal size and number of functional active zones at the calyx of held synapse by nonstationary EPSC variance analysis. *J Neurosci* 21:7889-7900.
- Mikaelian D, Ruben RJ (1964) Development of hearing in the normal CBA-J mouse. *Acta Otolaryngol* 59:451-461.
- Ming G, Wang LY (2003) Properties of voltage-gated sodium channels in developing auditory neurons of the mouse in vitro. *Chin Med Sci J* 18:67-74.
- Monyer H, Burnashev N, Laurie DJ, Sakmann B, Seeburg PH (1994) Developmental and regional expression in the rat brain and functional properties of four NMDA receptors. *Neuron* 12:529-540.
- Morest DK (1968) The growth of synaptic endings in the mammalian brain: a study of the calyces of the trapezoid body. *Z Anat Entwicklungsgesch* 127:201-220.
- Mu Y, Otsuka T, Horton AC, Scott DB, Ehlers MD (2003) Activity-dependent mRNA splicing controls ER export and synaptic delivery of NMDA receptors. *Neuron* 40:581-594.
- Muller D, Oliver M, Lynch G (1989) Developmental changes in synaptic properties in hippocampus of neonatal rats. *Brain Res Dev Brain Res* 49:105-114.
- Murthy VN, Schikorski T, Stevens CF, Zhu Y (2001) Inactivity produces increases in neurotransmitter release and synapse size. *Neuron* 32:673-682.
- Neher E, Sakaba T (2001a) Combining deconvolution and noise analysis for the estimation of transmitter release rates at the calyx of held. *J Neurosci* 21:444-461.
- Neher E, Sakaba T (2001b) Estimating transmitter release rates from postsynaptic current fluctuations. *J Neurosci* 21:9638-9654.
- O'Brien RJ, Kamboj S, Ehlers MD, Rosen KR, Fischbach GD, Huganir RL (1998) Activity-dependent modulation of synaptic AMPA receptor accumulation. *Neuron* 21:1067-1078.
- Oertel D (1999) The role of timing in the brain stem auditory nuclei of vertebrates. *Annu Rev Physiol* 61:497-519.
- Oleskevich S, Walmsley B (2002) Synaptic transmission in the auditory brainstem of normal and congenitally deaf mice. *J Physiol* 540:447-455.

- Oleskevich S, Clements J, Walmsley B (2000) Release probability modulates short-term plasticity at a rat giant terminal. *J Physiol* 524 Pt 2:513-523.
- Oleskevich S, Youssoufian M, Walmsley B (2004) Presynaptic plasticity at two giant auditory synapses in normal and deaf mice. *J Physiol* 560:709-719.
- Otsu Y, Shahrezaei V, Li B, Raymond LA, Delaney KR, Murphy TH (2004) Competition between phasic and asynchronous release for recovered synaptic vesicles at developing hippocampal autaptic synapses. *J Neurosci* 24:420-433.
- Pappas GD, Purpura DP, New York Society of Electron Microscopists. (1972) Structure and function of synapses. New York,: Raven Press.
- Perez-Otano I, Ehlers MD (2005) Homeostatic plasticity and NMDA receptor trafficking. *Trends Neurosci* 28:229-238.
- Pfeiffer RR, Kiang NY (1965) Spike Discharge Patterns of Spontaneous and Continuously Stimulated Activity in the Cochlear Nucleus of Anesthetized Cats. *Biophys J* 5:3.
- Philpot BD, Sekhar AK, Shouval HZ, Bear MF (2001) Visual experience and deprivation bidirectionally modify the composition and function of NMDA receptors in visual cortex. *Neuron* 29:157-169.
- Platzer J, Engel J, Schrott-Fischer A, Stephan K, Bova S, Chen H, Zheng H, Striessnig J (2000) Congenital deafness and sinoatrial node dysfunction in mice lacking class D L-type Ca²⁺ channels. *Cell* 102:89-97.
- Quinlan EM, Olstein DH, Bear MF (1999a) Bidirectional, experience-dependent regulation of N-methyl-D-aspartate receptor subunit composition in the rat visual cortex during postnatal development. *Proc Natl Acad Sci U S A* 96:12876-12880.
- Quinlan EM, Philpot BD, Hugarir RL, Bear MF (1999b) Rapid, experience-dependent expression of synaptic NMDA receptors in visual cortex in vivo. *Nat Neurosci* 2:352-357.
- Ramón y Cajal S (1911) *Histologie du système nerveux de l'homme & des vertébrés*, Éd. française rev. & mise à jour Edition. Madrid,: Consejo Superior de Investigaciones Científicas, Instituto Ramón y Cajal.
- Rao A, Craig AM (1997) Activity regulates the synaptic localization of the NMDA receptor in hippocampal neurons. *Neuron* 19:801-812.
- Reyes A, Sakmann B (1999) Developmental switch in the short-term modification of unitary EPSPs evoked in layer 2/3 and layer 5 pyramidal neurons of rat neocortex. *J Neurosci* 19:3827-3835.
- Roos J, Kelly RB (1999) The endocytic machinery in nerve terminals surrounds sites of exocytosis. *Curr Biol* 9:1411-1414.

- Rosenmund C, Clements JD, Westbrook GL (1993) Nonuniform probability of glutamate release at a hippocampal synapse. *Science* 262:754-757.
- Rowland KC, Irby NK, Spirou GA (2000) Specialized synapse-associated structures within the calyx of Held. *J Neurosci* 20:9135-9144.
- Rudy B, McBain CJ (2001) Kv3 channels: voltage-gated K⁺ channels designed for high-frequency repetitive firing. *Trends Neurosci* 24:517-526.
- Russell FA, Moore DR (1995) Afferent reorganisation within the superior olivary complex of the gerbil: development and induction by neonatal, unilateral cochlear removal. *J Comp Neurol* 352:607-625.
- Sahara Y, Takahashi T (2001) Quantal components of the excitatory postsynaptic currents at a rat central auditory synapse. *J Physiol* 536:189-197.
- Sakaba T (2006) Roles of the fast-releasing and the slowly releasing vesicles in synaptic transmission at the calyx of held. *J Neurosci* 26:5863-5871.
- Sakmann B, Neher E (1995) Single-channel recording, 2nd Edition. New York: Plenum Press.
- Sans N, Petralia RS, Wang YX, Blahos J, 2nd, Hell JW, Wenthold RJ (2000) A developmental change in NMDA receptor-associated proteins at hippocampal synapses. *J Neurosci* 20:1260-1271.
- Satzler K, Sohl LF, Bollmann JH, Borst JG, Frotscher M, Sakmann B, Lubke JH (2002) Three-dimensional reconstruction of a calyx of Held and its postsynaptic principal neuron in the medial nucleus of the trapezoid body. *J Neurosci* 22:10567-10579.
- Sätzler K, Sohl LF, Bollmann JH, Borst JG, Frotscher M, Sakmann B, Lubke JH (2002) Three-dimensional reconstruction of a calyx of Held and its postsynaptic principal neuron in the medial nucleus of the trapezoid body. *J Neurosci* 22:10567-10579.
- Schneggenburger R, Neher E (2000) Intracellular calcium dependence of transmitter release rates at a fast central synapse. *Nature* 406:889-893.
- Schneggenburger R, Forsythe ID (2006) The calyx of Held. *Cell Tissue Res*.
- Schneggenburger R, Meyer AC, Neher E (1999) Released fraction and total size of a pool of immediately available transmitter quanta at a calyx synapse. *Neuron* 23:399-409.
- Sheng M, Cummings J, Roldan LA, Jan YN, Jan LY (1994) Changing subunit composition of heteromeric NMDA receptors during development of rat cortex. *Nature* 368:144-147.
- Sherrington CS (1906) The integrative action of the nervous system. New York,: C. Scribner's sons.

- Shi J, Aamodt SM, Constantine-Paton M (1997) Temporal correlations between functional and molecular changes in NMDA receptors and GABA neurotransmission in the superior colliculus. *J Neurosci* 17:6264-6276.
- Smith PH, Joris PX, Carney LH, Yin TC (1991) Projections of physiologically characterized globular bushy cell axons from the cochlear nucleus of the cat. *J Comp Neurol* 304:387-407.
- Song P, Yang Y, Barnes-Davies M, Bhattacharjee A, Hamann M, Forsythe ID, Oliver DL, Kaczmarek LK (2005) Acoustic environment determines phosphorylation state of the Kv3.1 potassium channel in auditory neurons. *Nat Neurosci* 8:1335-1342.
- Spirou GA, Brownell WE, Zidanic M (1990) Recordings from cat trapezoid body and HRP labeling of globular bushy cell axons. *J Neurophysiol* 63:1169-1190.
- Stocca G, Vicini S (1998) Increased contribution of NR2A subunit to synaptic NMDA receptors in developing rat cortical neurons. *J Physiol* 507 (Pt 1):13-24.
- Sudhof TC (2004) The synaptic vesicle cycle. *Annu Rev Neurosci* 27:509-547.
- Takahashi T, Feldmeyer D, Suzuki N, Onodera K, Cull-Candy SG, Sakimura K, Mishina M (1996) Functional correlation of NMDA receptor epsilon subunits expression with the properties of single-channel and synaptic currents in the developing cerebellum. *J Neurosci* 16:4376-4382.
- Taschenberger H, von Gersdorff H (2000) Fine-tuning an auditory synapse for speed and fidelity: developmental changes in presynaptic waveform, EPSC kinetics, and synaptic plasticity. *J Neurosci* 20:9162-9173.
- Taschenberger H, Scheuss V, Neher E (2005) Release kinetics, quantal parameters and their modulation during short-term depression at a developing synapse in the rat CNS. *J Physiol* 568:513-537.
- Taschenberger H, Leao RM, Rowland KC, Spirou GA, von Gersdorff H (2002) Optimizing synaptic architecture and efficiency for high-frequency transmission. *Neuron* 36:1127-1143.
- Teng H, Wilkinson RS (2000) Clathrin-mediated endocytosis near active zones in snake motor boutons. *J Neurosci* 20:7986-7993.
- Thiagarajan TC, Piedras-Renteria ES, Tsien RW (2002) alpha- and betaCaMKII. Inverse regulation by neuronal activity and opposing effects on synaptic strength. *Neuron* 36:1103-1114.
- Thiagarajan TC, Lindskog M, Tsien RW (2005) Adaptation to synaptic inactivity in hippocampal neurons. *Neuron* 47:725-737.
- Tian N, Copenhagen DR (2001) Visual deprivation alters development of synaptic function in inner retina after eye opening. *Neuron* 32:439-449.

- Tollin DJ (2003) The lateral superior olive: a functional role in sound source localization. *Neuroscientist* 9:127-143.
- Tovar KR, Westbrook GL (1999) The incorporation of NMDA receptors with a distinct subunit composition at nascent hippocampal synapses in vitro. *J Neurosci* 19:4180-4188.
- Townsend M, Liu Y, Constantine-Paton M (2004) Retina-driven dephosphorylation of the NR2A subunit correlates with faster NMDA receptor kinetics at developing retinocollicular synapses. *J Neurosci* 24:11098-11107.
- Townsend M, Yoshii A, Mishina M, Constantine-Paton M (2003) Developmental loss of miniature N-methyl-D-aspartate receptor currents in NR2A knockout mice. *Proc Natl Acad Sci U S A* 100:1340-1345.
- Trussell LO (1999) Synaptic mechanisms for coding timing in auditory neurons. *Annu Rev Physiol* 61:477-496.
- Turrigiano GG, Nelson SB (2004) Homeostatic plasticity in the developing nervous system. *Nat Rev Neurosci* 5:97-107.
- Turrigiano GG, Leslie KR, Desai NS, Rutherford LC, Nelson SB (1998) Activity-dependent scaling of quantal amplitude in neocortical neurons. *Nature* 391:892-896.
- Vale C, Sanes DH (2000) Afferent regulation of inhibitory synaptic transmission in the developing auditory midbrain. *J Neurosci* 20:1912-1921.
- Van der Kloot W (1988) Estimating the timing of quantal releases during end-plate currents at the frog neuromuscular junction. *J Physiol* 402:595-603.
- von Gersdorff H, Borst JG (2002) Short-term plasticity at the calyx of held. *Nat Rev Neurosci* 3:53-64.
- Wang LY, Kaczmarek LK (1998) High-frequency firing helps replenish the readily releasable pool of synaptic vesicles. *Nature* 394:384-388.
- Watt AJ, van Rossum MC, MacLeod KM, Nelson SB, Turrigiano GG (2000) Activity coregulates quantal AMPA and NMDA currents at neocortical synapses. *Neuron* 26:659-670.
- Wierenga CJ, Walsh MF, Turrigiano GG (2006) Temporal Regulation of the Expression Locus of Homeostatic Plasticity. *J Neurophysiol*.
- Williams K (1993) Ifenprodil discriminates subtypes of the N-methyl-D-aspartate receptor: selectivity and mechanisms at recombinant heteromeric receptors. *Mol Pharmacol* 44:851-859.
- Williams K, Russell SL, Shen YM, Molinoff PB (1993) Developmental switch in the expression of NMDA receptors occurs in vivo and in vitro. *Neuron* 10:267-278.

- Wilson NR, Kang J, Hueske EV, Leung T, Varoqui H, Murnick JG, Erickson JD, Liu G (2005) Presynaptic regulation of quantal size by the vesicular glutamate transporter VGLUT1. *J Neurosci* 25:6221-6234.
- Wimmer VC, Nevian T, Kuner T (2004) Targeted in vivo expression of proteins in the calyx of Held. *Pflugers Arch* 449:319-333.
- Wimmer VC, Horstmann H, Groh A, Kuner T (2006) Donut-like topology of synaptic vesicles with a central cluster of mitochondria wrapped into membrane protrusions: a novel structure-function module of the adult calyx of Held. *J Neurosci* 26:109-116.
- Wölfel M (2004) Analysis of two kinetically distinct components of transmitter release at a fast synapse of the mammalian central nervous system. In: PhD Thesis.
- Wu LG, Borst JG, Sakmann B (1998) R-type Ca²⁺ currents evoke transmitter release at a rat central synapse. *Proc Natl Acad Sci U S A* 95:4720-4725.
- Wu LG, Westenbroek RE, Borst JG, Catterall WA, Sakmann B (1999) Calcium channel types with distinct presynaptic localization couple differentially to transmitter release in single calyx-type synapses. *J Neurosci* 19:726-736.
- Wu SH, Kelly JB (1993) Response of neurons in the lateral superior olive and medial nucleus of the trapezoid body to repetitive stimulation: intracellular and extracellular recordings from mouse brain slice. *Hear Res* 68:189-201.
- Yamashita T, Ishikawa T, Takahashi T (2003) Developmental increase in vesicular glutamate content does not cause saturation of AMPA receptors at the calyx of held synapse. *J Neurosci* 23:3633-3638.
- Yamashita T, Hige T, Takahashi T (2005) Vesicle endocytosis requires dynamin-dependent GTP hydrolysis at a fast CNS synapse. *Science* 307:124-127.
- Youssoufian M, Oleskevich S, Walmsley B (2005) Development of a robust central auditory synapse in congenital deafness. *J Neurophysiol* 94:3168-3180.

ACKNOWLEDGMENTS

I want to thank my research advisor Dr. Holger Taschenberger for a great supervision and tremendous teaching. Thanks for showing me how to patch!

I am grateful to Prof. Dr. Erwin Neher, Prof. Dr. Walter Stühmer and Prof. Dr. Tobias Moser for their assistance, support and discussions during my thesis committee meetings.

Special thanks to all the members of the department, especially to Dr. Takeshi Sakaba and Dr. Nobutake Hosoi for very helpful comments on my work. Special thanks also to Irmgard Barteczko for helping me with all the administrative issues of being a PhD student.

For reading and commenting this manuscript I want to thank infinitely to Natalia Mackenzie – without you I'm nothing! Thanks for all your support and for the motivation that you gave me all this years.

I would like to acknowledge Dr. Steffen Burkhardt, Dr. Simone Cardoso de Oliveira, Sandra Drube, Prof. Dr. Michael Hörner and Dr. Dorothee Wegener and all the people involved in the coordination and realization of the neuroscience program in Göttingen.

I would also like to express my gratitude to the Graduiertenkolleg Neuroplasticity from Molecules to Systems and the Deutsche Forschungsgemeinschaft for their support. Here, I particularly want to thank Christine Crozier for taking care of wonderful Summer schools, and Prof. Dr. Walter Paulus.

I also want to express my gratitude to all my friends here in Göttingen – especially Dr. Martin Wienisch for great support during the writing of this work.

The greatest thanks appertain to my parents Inge Fischer and Ricardo Erazo. Without their support I would not be here.

CURRICULUM VITAE

Emilio Erazo Fischer

Am Fassberg 11, 37077 Göttingen

0551 2011676

emilio.fischer@mpi-bpc.mpg.deBorn on 19th July 1976 in Punta Arenas, Chile

Nationality: Chilean and German

Education

*Universidad de Chile, Santiago, Chile***Molecular Biotechnology Engineering****1996-2001***University of Göttingen, Germany***International Max-Planck School in Neurosciences****2002-2003***Max-Planck Institute for Biophysical Chemistry***PhD student****Department of Membrane Biophysics****2003-today**

Scholarships

- Stipend International Max-Planck Research School **2002 – 2003**
- Stipend from the Deutsche Forschungsgemeinschaft (DFG) **2003 – today**

LIST OF PUBLICATIONS

Erazo-Fischer E, Taschenberger H.

The role of physiological afferent nerve activity during *in-vivo* maturation of the calyx of Held synapse.

(submitted)